Cellular/Molecular

Role of Voltage-Gated K^+ Channels and K2P Channels in Intrinsic Electrophysiological Properties and Saltatory Conduction at Nodes of Ranvier of Rat Lumbar Spinal Ventral Nerves

Sotatsu Tonomura and Jianguo G. Gu

Department of Anesthesiology and Perioperative Medicine, School of Medicine, University of Alabama at Birmingham, Birmingham, Alabama 35294

Ion channels at the nodes of Ranvier (NRs) are believed to play essential roles in intrinsic electrophysiological properties and saltatory conduction of action potentials (AP) at the NRs of myelinated nerves. While we have recently shown that two-pore domain potassium (K2P) channels play a key role at the NRs of Aβ-afferent nerves, K^+ channels and their functions at the NRs of mammalian motor nerves remain elusive. Here we addressed this issue by using *ex vivo* preparations of lumbar spinal ventral nerves from both male and female rats and the pressure-patch-clamp recordings at their NRs. We found that depolarizing voltages evoked large noninactivating outward currents at NRs. The outward currents could be partially inhibited by voltage-gated K^+ channel blockers, largely inhibited by K2P blockers and cooling temperatures. Inhibition of the outward currents by voltage-gated K^+ channel blockers, K2P blockers, or cooling temperatures significantly altered electrophysiological properties measured at the NRs, including resting membrane potential, input resistance, AP width, AP amplitude, AP threshold, and AP rheobase. Furthermore, K2P blockers and cooling temperatures significantly reduced saltatory conduction velocity and success rates of APs in response to high-frequency stimulation. Voltage-gated K^+ channel blockers reduced AP success rates at high-frequency stimulation without significantly affecting saltatory conduction velocity. Collectively, both K2P and voltage-gated K^+ channels play significant roles in intrinsic electrophysiological properties and saltatory conduction at NRs of motor nerve fibers of rats. The effects of cooling temperatures on saltatory conduction are at least partially mediated by K2P channels at the NRs.

Key words: **action potential; node of Ranvier; patch-clamp recording; saltatory conduction; two-pore domain K^+ channel; voltage-gated K^+ channel**

Significance Statement

Ion channels localized at the NRs are believed to be key determinants of saltatory conduction on myelinated nerves. However, ion channels and their functions at the NRs have not been fully studied in different types of mammalian myelinated nerves. Here we use the pressure-patch-clamp recordings to show that both K2P and voltage-gated K^+ channels play significant roles in intrinsic electrophysiological properties and saltatory conduction at NRs of lumbar spinal ventral nerves of rats. Furthermore, cooling temperatures exert effects on saltatory conduction via inhibition of ion channels at the NRs. Our results provide new insights into saltatory conduction on myelinated nerves and may have physiological as well as pathologic implications.

Introduction

Action potential (AP) propagation through nodes of Ranvier (NRs) along myelinated nerves, known as saltatory conduction (Ranvier, 1871, 1872; Lillie, 1925; Tasaki, 1939; Huxley and Stampfli, 1949; Boullerne, 2016), is essential for timely sensory responses with high acuity and rapid muscle movement with fine control. Saltatory conduction can reach speeds over 100 m/s and frequencies over hundreds of Hertz, 100 times more rapid than impulse conduction on unmyelinated nerves in mammals (Waddell and Lawson, 1990). Impairment

Received Mar. 14, 2022; revised May 2, 2022; accepted May 17, 2022.

Author contributions: J.G.G. designed research; J.G.G. edited the paper; J.G.G. wrote the paper; S.T. performed research; S.T. analyzed data; S.T. wrote the first draft of the paper.

This work was supported by National Institutes of Health Grants NS109059, DE018661, and DE023090 to J.G.G. We thank Dr. Ryan Vaden for reading and commenting on the previous version of this manuscript.

The authors declare no competing financial interests.

Correspondence should be addressed to Jianguo G. Gu at jianguogu@uabmc.edu.

https://doi.org/10.1523/JNEUROSCI.0514-22.2022

of saltatory conduction at NRs occurs in many neurologic diseases, including multiple sclerosis, spinal cord injury, and inflammatory demyelinating polyneuropathy (Waxman, 1992, 2006; Devaux et al., 2012; Arancibia-Carcamo and Attwell, 2014; Stathopoulos et al., 2015), leading to sensory and motor dysfunctions. NRs are the only sites on myelinated nerves where APs can be regenerated for saltatory conduction. Ion channels localized at the NRs are thought to be key determinants of intrinsic electrophysiological properties and saltatory conduction at the NRs, and believed to have important physiological and pathologic implications. However, ion channels and their functions at the NRs have not been fully studied in different types of mammalian myelinated nerves.

AP regeneration and conduction at NRs of myelinated nerves have long been thought to use the same ion channel mechanism as that in the other parts of nerves; that is, AP depolarization is driven by voltage-gated Na^+ channels and AP repolarization driven mainly by voltage-gated K^+ channels (Hodgkin and Huxley, 1952; Bean, 2007). Indeed, this classical ion channel mechanism largely underlies AP regeneration and propagation at amphibian NRs (Hille, 1967; Hucho et al., 1976). On myelinated nerves of mammals, immunohistochemical studies have shown that Nav1.6 voltage-gated Na^+ channels are highly clustered at NRs (Caldwell et al., 2000; Waxman, 2006). These channels are believed to drive membrane depolarization to regenerate APs at the NRs (Caldwell et al., 2000). Interestingly, in mammalian species, including rats and rabbits, Chiu and Ritchie (1980, 1981) failed to detect significant K^+ currents at intact NRs of mammals, except when the myelin sheaths of the nerves were chemically loosen, and they suggested that K^+ channels were not present at intact mammalian NRs. On the other hand, Binah and Palti (1981) detected large K^+ currents at NRs of rat myelinated nerves. Since then, there have been long debates on whether or not K^+ channels are present at NRs for AP regeneration and conduction at NRs. Using immunohistochemical approaches, Kv7.2 (Devaux et al., 2004) and Kv3.1b (Devaux et al., 2003) voltage-gated K^+ channels were detected at mammalian NRs, and Kv1.1 as well as Kv1.2 voltage-gated K^+ channels were detected in juxtaparanodal regions (Rhodes et al., 1997). However, roles of these voltage-gated K^+ channels in intrinsic electrophysiology properties and saltatory conduction at mammalian NRs remain largely unclear since it has been technically challenging to perform patch-clamp recordings at the NRs of mammalian nerves.

Only recently has it become possible to directly study ion channels and their functions at mammalian NRs by recently developed pressure-patch-clamp recording technique (Kanda et al., 2019, 2021a). Applying this technique to the NRs of rat trigeminal Aβ-afferent nerves, we have shown that TREK-1 and TRAAK, the thermosensitive and mechanosensitive two-pore domain potassium (K2P) channels, are principal K^+ channels clustered at mammalian NRs of somatosensory nerves. Consistently, immunohistochemical studies have shown strong TREK-1 and TRAAK immunoreactivity clustered at mammalian NRs of different nerves, including somatosensory nerves (Brohawn et al., 2019; Kanda et al., 2019). K2P channels are a family of 15 members that are originally known as "leak" or "background" K^+ channels (Goldstein et al., 2005; Lotshaw, 2007; Enyedi and Czirjak, 2010). K2P channels are distinct from voltage-gated K^+ channels in their structure, biophysical and pharmacological properties, and electrophysiological functions (Enyedi and Czirjak, 2010). K2P channels are expressed at low levels on somas of neurons and contribute to setting membrane input conductance and resting membrane potential (RMP) (Enyedi and Czirjak, 2010). We have found that K2P channels, but not voltage-gated K^+ channels, are involved in intrinsic electrophysiological properties and AP regeneration at the NRs of somatosensory nerves (Kanda et al., 2019, 2021b). Furthermore, we have shown that K2P channels permit high-speed and high-frequency AP conduction along somatosensory nerves (Kanda et al., 2019). Our immunohistochemical study has also shown strong TREK-1 immunoreactivity clustered at the NRs of motor nerves of rats (Kanda et al., 2019). In addition, strong TRAAK immunoreactivity has been observed at the NRs of mouse sciatic nerves (Brohawn et al., 2019). However, functions of K2P channels and voltage-gated K^+ channels at the NRs of mammalian motor nerves have so far not been studied using the patch-clamp recording technique.

Materials and Methods

Ex vivo *lumbar spinal ventral nerve preparation.* Sprague Dawley rats of both males and females 6-14 weeks of age were deeply anesthetized with isoflurane and killed by decapitation. Lumbar L4 or L5 spinal ventral nerves each at the length of ~20 mm were dissected out and placed in a Petri dish filled with Krebs solution that contained the following (in mM): 117 NaCl, 3.5 KCl, 2.5 $CaCl_2$, 1.2 $MgCl_2$, 1.2 NaH_2PO_4, 25 $NaHCO_3$, and 11 glucose. The Krebs solution was saturated with 95% O_2 and 5% CO_2, had pH of 7.35 and osmolarity of 324 mOsm, and at room temperature of ~24°C. Connective tissues on the surface of the nerve bundles were removed with a pair of fine forceps under a dissection microscope, then affixed in a recording chamber by a tissue anchor and submerged in the Krebs solution. The recording chamber was mounted on the stage of an Olympus BX51 microscope that was equipped with IR-DIC and fluorescent imaging systems. To facilitate the penetration of patch-clamp electrode through perineural tissues, the lumbar spinal ventral nerves were briefly exposed to a mixture of 0.07% dispase II (Roche) and 0.07% collagenase (Millipore Sigma) in the Krebs solution for 5-10 min at room temperature, and the enzymes were then washed off with the Krebs solution. The *ex vivo* nerve preparation was continuously perfused with the Krebs solution at 24°C maintained by a Peltier temperature control system (CL-200A, Warner Instrument).

Morphology of NRs and internodal axons of lumbar spinal ventral nerves. To determine lengths and diameters of nodal axons and internodal axons, axons were labeled by the fluorescent dye AlexaFluor-555 dye (Thermo Fisher Scientific). The dye was included in recording electrode internal solution at a final concentration of 85 μM. Pressure-patch-clamp was applied to the NR (see Pressure-patch-clamp recordings at NRs), and following the establishment of the whole-cell configuration for 30 min, nodal and internodal axons filled with AlexaFluor-555 were visualized under the fluorescent light. The fluorescence excitation was provided by an LED illumination system (X-Cite 120 LED, Lumen Dynamics). A filter set with excitation wavelength of 500-550 nm and emission wavelength of 565-625 nm was used for imaging AlexaFluor-555 fluorescence. The images of dye-labeled axons were captured with a digital complementary metal-oxide semiconductor (CMOS) camera (ORCA-Flash 4.0, Hamamatsu). The images were then analyzed using the ImageJ software (National Institutes of Health) to measure the lengths and diameters of nodal, paranodal, and internodal axons.

Pressure-patch-clamp recordings at NRs. NRs in lumbar spinal ventral nerves were visualized under a 40× (NA 0.80) water immersion objective with live images captured by an infrared CCD camera (IR-1000, DAGE-MTI). Patch-clamp recordings were performed at the NRs of lumbar spinal ventral nerves. Recording electrodes were pulled with a Flaming/Brown Micropipette Puller (P-97, Sutter Instruments). The electrode resistance after filling recording electrode internal solutions ranged from 5 to 8 MΩ for patch-clamp recordings at NRs. For most experiments, recording electrodes were filled with a K^+-based internal solution containing the following (in mM): 105 K-gluconate, 30 KCl, 0.5 $CaCl_2$, 2.4 $MgCl_2$, 5 EGTA, 10 HEPES, 5 Na_2ATP, and 0.33 GTP-TRIS salt; the pH of the solution was adjusted to 7.35 with KOH. In a different set of experiments, a Cs^+-based recording electrode internal solution

was used and the solution contained the following (in mM): 135 CsCl, 0.5 $CaCl_2$, 2.4 $MgCl_2$, 1 4-aminopyridine (4-AP), 5 EGTA, 10 HEPES, 5 Na_2ATP, and 0.33 GTP-TRIS salt; the pH of the solution was adjusted to 7.35 with CsOH. In the Cs^+-based recording electrode internal solution, Cs^+ served as a major intracellular cation and also as a blocker for voltage-gated K^+ channels. To access nodal axon membranes by recording electrodes and achieve high-quality membrane seals, a high-speed pressure-clamp device (HSPC-1, ALA Scientific Instruments) was connected to the patch-clamp recording electrode holder to finely control internal pressures of patch-clamp recording electrodes while approaching nodal membranes. The pressure-patch-clamp recordings were performed in the same manner as those described in our previous studies (Kanda et al., 2019, 2021a,b). Signals of voltage-clamp experiments were recorded and amplified using a multiclamp 700B amplifier, filtered at 10 kHz and sampled at 10 kHz using the pCLAMP 11 software (Molecular Devices). Signals of current-clamp recordings for APs at NRs were low-pass filtered at 10 kHz and sampled at 50 kHz.

To measure ionic currents flowing through nodal membranes following voltage steps, recordings were performed under the whole-cell voltage-clamp configuration with nodal membranes held at −72 mV. Voltage steps were applied from −112 to 58 mV (voltage command of −100 to 70 mV) with increments of 10 mV each step and a step duration of 500 ms. Unless otherwise indicated, membrane voltages mentioned in the text have been corrected for the calculated junction potentials of 12.3 mV for the recording electrode internal solution with 135 mM K^+ and of 4.3 mV for the recording electrode internal solution with 135 mM CsCl. To determine the properties of membranes and APs at the NRs, patch-clamp recordings were performed under the whole-cell current-clamp configuration with bridge balance being applied during recordings. Step currents were injected into NRs through recording electrodes. Step currents were applied from −100 to 2000 pA with increments of 50 pA per step, and the duration of each step was 500 ms.

Determination of saltatory conduction velocity (CV) and AP success rates at NRs of lumbar spinal ventral nerves. To determine conduction velocity of APs propagated through NRs on lumbar spinal ventral nerves, APs were orthodromically evoked using a suction stimulation electrode. The distance between the stimulation sites and the recording site was ~15 mm. The tip of the suction stimulation electrode was ~0.5 mm in diameter and was fire-polished. The end of the nerve bundle was aspirated into the suction stimulation electrode to produce a tight fitting by negative pressure. The negative pressure was continuously applied into the suction stimulation electrode to maintain the tight fitting during experiments. To initiate APs at the end of the nerve bundle, monophasic square wave pulses were generated by an electronic stimulator (Master-8, A.M.P.I.) and delivered via a stimulation isolator (ISO-Flex, A.M.P.I.) to the suction stimulation electrode. The duration of the stimulation pulse was 50 µs. Stimulation threshold of the nerve (i.e., the minimum stimulation intensity for evoking APs) was first determined and was ~100 µA. Then stimulation was applied at the intensity of twofold threshold throughout the experiments. CV was calculated based on the latency of APs and the length of nerve fibers. The latency of APs was measured from the time of stimulation that was marked by stimulation artifacts

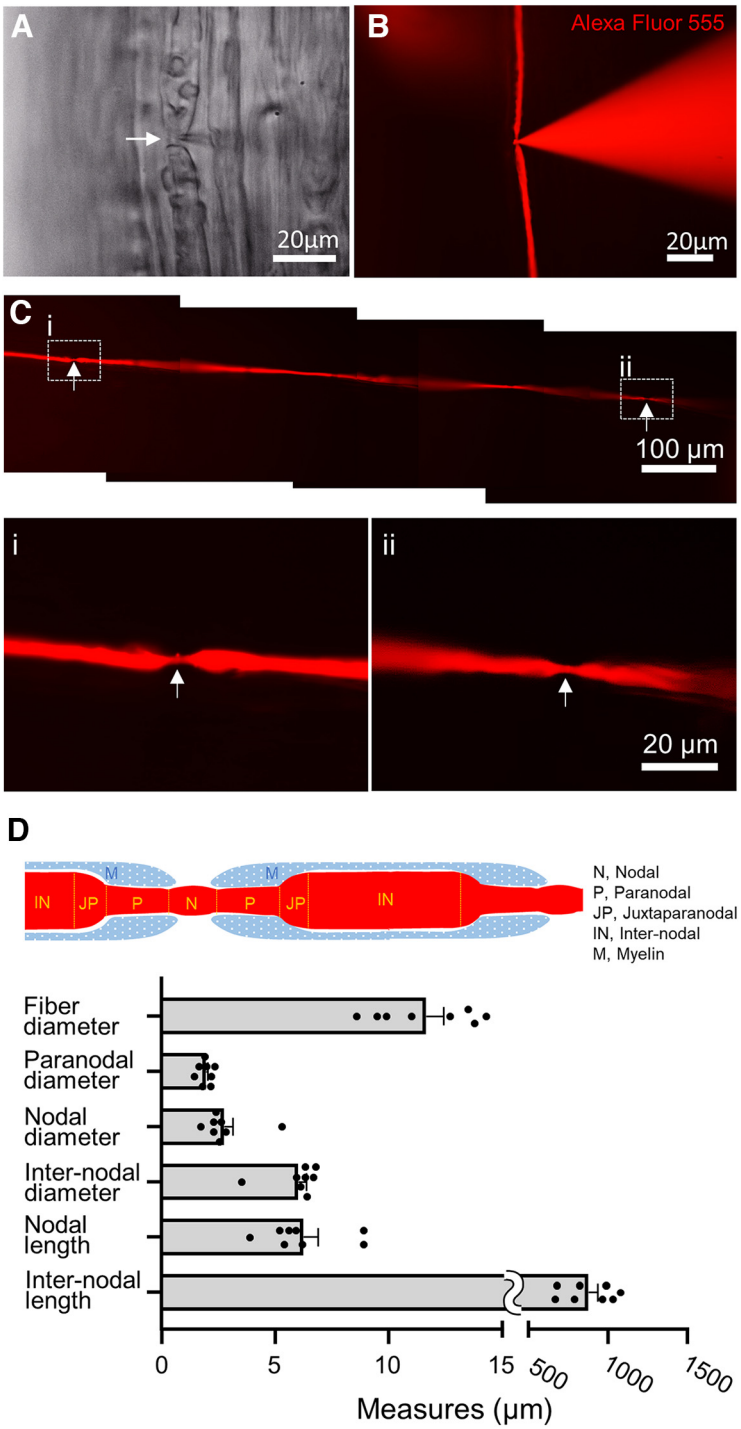

Figure 1. Morphology of the nodal and intermodal axons of freshly prepared *ex vivo* lumbar spinal ventral nerves. ***A***, Bright field image represents a region of a fresh *ex vivo* preparation of L5 lumbar spinal ventral nerve viewed under a 40× objective. Arrow indicates an NR on a nerve fiber. To the right side of the arrow, there is a patch-clamp recording electrode whose tip is on the NR. ***B***, Fluorescent image of the same field of ***A*** shows the axon vitally labeled by AlexaFluor-555 following the whole-cell patch-clamp recording. AlexaFluor-555 (85 µM) was included in the recording electrode internal solution. ***C***, A series of fluorescent images of AlexaFluor-555-labeled axon that was distal from the recording site (not shown). Arrows indicate two NRs on the axon. Two regions in the box ***Ci*** and ***Cii*** are enlarged and displayed below to show two NRs each with narrower axon. ***D***, Top, Diagram represents morphologic components of a myelinated nerve. Bottom, Morphologic parameters ($n = 8$) of nodal, paranodal, and internodal axons of fresh lumbar spinal ventral nerves following AlexaFluor-555-labeling. Data are mean ± SEM.

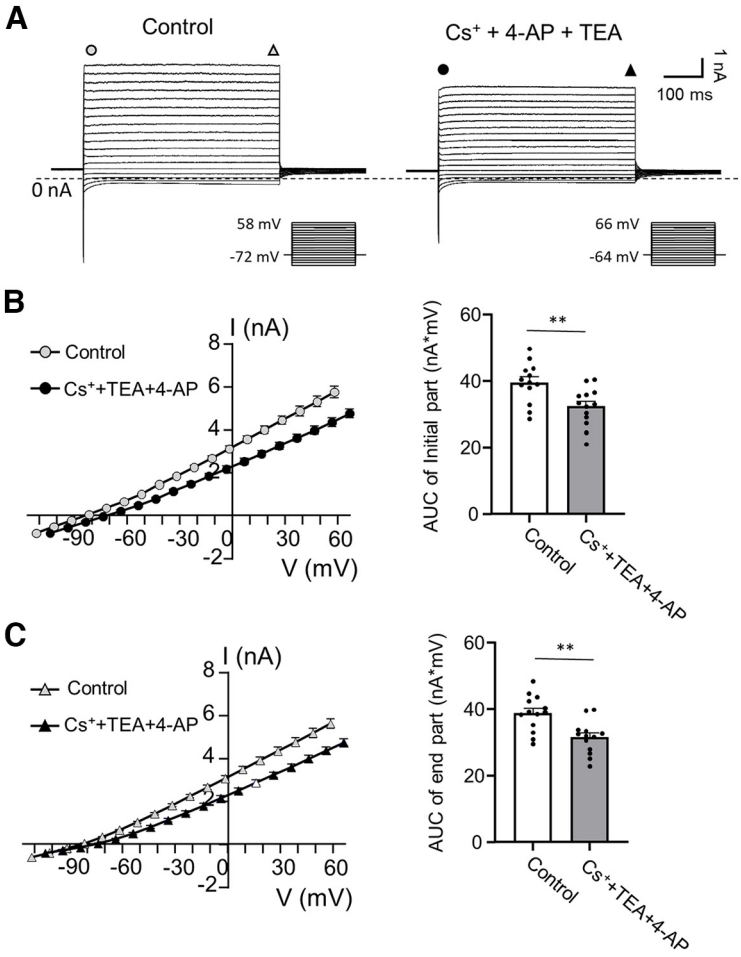

Figure 2. NRs of lumbar spinal ventral nerves represent a high level of leak K^+ currents and a low level of voltage-gated K^+ currents. ***A***, Two sets of sample traces represent currents recorded at an NR following voltage steps in the absence (left, control) and presence of voltage-gated K^+ channel blockers Cs^+ + 4-AP + TEA (right). Circles and triangles represent the initial and the end components of the currents, respectively. Currents at these two places are used to plot *I–V* relationship in ***B*** and ***C***. Voltage commands are shown under each set of the sample current traces. ***B***, Left, *I–V* curves of noninactivating currents of the initial component in control ($n = 13$) and the presence of Cs^+ + 4-AP + TEA ($n = 13$). Right, AUC of the noninactivating currents of the initial component in control ($n = 13$) and the presence of Cs^+ + 4-AP + TEA ($n = 13$). ***C***, Left, *I–V* curves of noninactivating currents of the end component in control ($n = 13$) and the presence of Cs^+ + 4-AP + TEA ($n = 13$). Right, AUC of the noninactivating currents of the end component in control ($n = 12$) and the presence of Cs^+ + 4-AP + TEA ($n = 13$). AUCs were used for statistical comparison of noninactivating currents in control and the presence of Cs^+ + 4-AP + TEA. In experiments with voltage-gated K^+ channel blockers, 135 mM Cs^+ plus 1 mM 4-AP were applied intracellularly, and 20 mM TEA was applied extracellularly. Data are mean ± SEM. $^{**}p < 0.01$ (Student's *t* test).

to the time when AP was initiated at the recording site. The length of the nerve fiber was the distance between stimulation site and the recording site. To determine success rates of APs at the NRs following different stimulation frequencies, stimulation pulses were applied to the nerve bundles at frequencies of 1, 10, 50, 100, 200, 500, and 1000 Hz. Stimulation at each frequency was applied for 20 s. Intervals between different tests were 30 s. Success rates of APs conducted through the NRs were defined as the percentage of successfully propagated APs through the nodal recording sites during 20 s period of stimulation.

Pharmacology. Effects on intrinsic electrophysiological properties of NRs by compounds that blocked voltage-gated K^+ and K2P channels were examined. Blockers of voltage-gated K^+ channels tested in this set of experiments included tetraethylammonium (TEA, 20 mM, Millipore Sigma), 4-AP (1 mM, Millipore Sigma), and cesium (Cs^+, 135 mM, Millipore Sigma). 4-AP and Cs^+ were applied intracellularly, and 135 mM Cs^+ replaced 135 mM K^+ in the recording electrode internal solution. Testing compounds with blocking effects on K2P channels included barium (Ba^{2+}, 5 mM, Millipore Sigma), ruthenium red (RR, 200 μM, Millipore Sigma), norfluoxetine (NF, 50 and 250 μM, Cayman Chemical, mibefradil (10 μM, Millipore Sigma), amlodipine (100 μM, Tocris Bioscience), gadolinium (Gd^{3+}, 50 μM, Millipore Sigma), spadin (1 μM, Millipore Sigma), chlopromazine (100 μM, Millipore Sigma), diltiazem (1 mM, Millipore Sigma), and bupivacaine (3 mM, Millipore Sigma). In addition to the aforementioned testing compounds, TTX (500 nM, Tocris Bioscience) was tested for its blocking effect on voltage-gated Na^+ channels. Unless otherwise indicated, testing compounds were bath-applied. For all pharmacology tests with bath application of testing compounds, unless otherwise indicated, each compound was perfused to *ex vivo* nerve preparations for 10 min.

Effects of temperatures. Effects of temperatures on intrinsic electrophysiological properties at NRs as well as on saltatory conductions of APs through NRs along lumbar spinal ventral nerves were investigated by the aforementioned electrophysiological experiments at bath solution temperatures of 35°C, 24°C, and 15°C. The temperatures of bath solutions were controlled by a Peltier temperature control system (CL-200A, Warner Instrument), and were continuously monitored with a thermal probe placed in the recording chamber (TA-29, Warner Instrument). The bath solution was applied at 2 ml/min from a short tube (500 μm in internal diameter) whose outlet was positioned 1 cm away from the recording site. The time was <1 min for warming from 24°C to 35°C and <1 min for cooling from 24°C to 15°C at the recording site.

Data analysis. Electrophysiological data were measured using Clampfit 11 (Molecular Devices). Data were collected from L4 and L5 lumbar spinal ventral nerves of 33 male and 23 female animals, and were aggregated for data analysis since no significant differences in electrophysiological results were found between male and female animals. Input resistance was determined with a −10 mV voltage step from the membrane holding voltage of −72 mV. RMP was measured under current-clamp configuration at the zero holding current. AP rheobase was the threshold step current that evoked AP firing. AP threshold was the potential at which AP upstroke started. AP amplitude was measured from RMP to AP peak. AP width was measured as the duration from 50% AP upstroke to 50% AP repolarization. All the above AP parameters were determined with the AP evoked by the rheobase step current at the NR. AP success rates at the NRs were calculated as the number of APs recorded at the NRs divided by the number of electrical stimuli, where the electrical stimuli were applied to the lumbar spinal ventral nerves at different frequencies for 20 s. Curve-fitting was performed using a nonlinear regression fit with the following equation: $Y=100/(1+10\text{^}((\text{LogIC50} - X) \times \text{Hill Slope}))$, where Y is normalized response (AP success rate), X is variable (stimulation frequency), IC_{50} is stimulation frequency at which success rate is 50% (FS_{50}). All data analyses were performed using Graph Pad Prism (version 8). Analysis for normality was performed with the Shapiro–Wilk test for each set of data before statistical analysis, and all data were normally distributed. Unless otherwise indicated, all data were reported as mean ± SEM of *n* independent observations. Statistical significance was evaluated using one-way ANOVA with Tukey's *post hoc* tests or Student's *t* tests.

Results

Axon morphology of freshly prepared lumbar spinal ventral nerves

Under a 40× objective in bright field, individual nerve fibers and their NRs could be visualized in lumbar spinal ventral nerves. The diameters of these nerve fibers with their myelin sheath were 11.7 ± 0.8 µm ($n = 8$, Fig. 1*A*,*D*). However, axons at the NRs and internodal regions could not be directly visualized in the bright field because of heavy myelination. In our experiments with pressure-patch-clamp recordings, we labeled axons by including the fluorescent dye AlexaFluor-555 in recording electrode internal solution. Under a fluorescent microscope, we could visualize fluorescence-labeled axons of freshly prepared lumbar spinal ventral nerves (Fig. 1*B*). Axons at NRs were much narrower than internodal axons (Fig. 1*C*). In eight nerve fibers sampled, the diameters of NRs and the paranodal region were 2.7 ± 0.4 µm ($n = 8$) and 1.9 ± 0.1 µm ($n = 8$, Fig. 1*D*), respectively. The diameter of internodal axons was 6.0 ± 0.4 µm ($n = 8$, Fig. 1*D*). The length of nodal axons and internodal axons was 6.3 ± 0.6 µm ($n = 8$) and 878.5 ± 56.3 µm ($n = 8$), respectively (Fig. 1*D*).

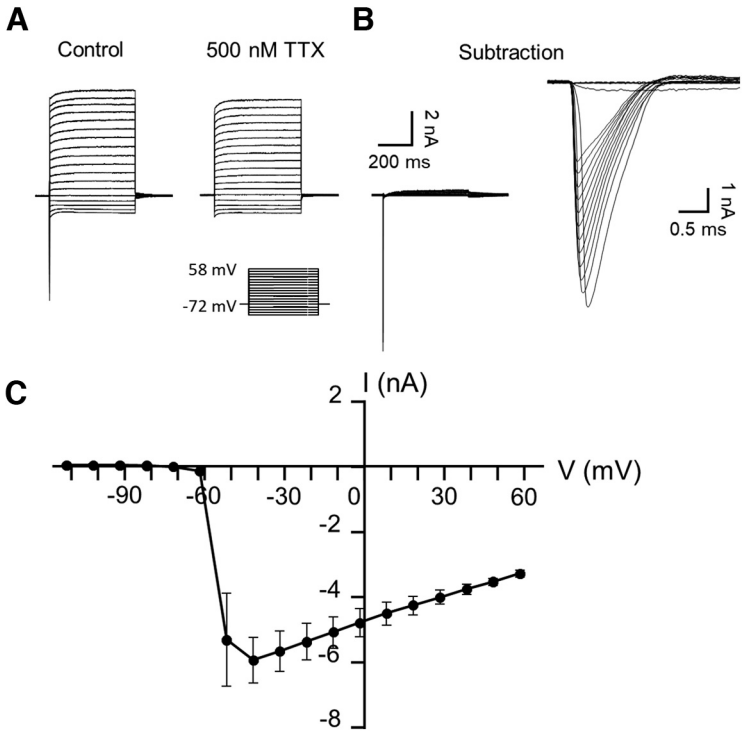

Figure 3. Transient inward currents evoked at the NR of lumbar spinal ventral nerves and their sensitivity to TTX. ***A***, Sample traces represent currents recorded at an NR following voltage steps in the absence (control, left) and presence of voltage-gated Na^+ channel blocker TTX (500 nM, right). Voltage commands are shown under the sample current traces. ***B***, Left, TTX-sensitive inward currents obtained by subtraction of total currents in TTX from total currents in the control. Right, TTX-sensitive inward currents displayed in an expanded time scale. ***C***, Current–voltage relationship (*I–V* curve) of TTX-sensitive voltage-activated Na^+ currents recorded at NRs of lumbar spinal ventral nerves ($n = 5$). Data are mean ± SEM.

Ionic currents evoked by depolarizing voltages at the NRs of lumbar spinal ventral nerves

Under voltage-clamp configuration, we examined membrane currents evoked by depolarizing voltage steps at NRs of lumbar spinal ventral nerves (Fig. 2). Depolarizing voltage steps evoked large transient inward currents immediately followed by large noninactivating outward currents (Fig. 2*A*, left) in the control group without voltage-gated K^+ channel blockers. The noninactivating outward currents at the NRs reversed at −84.6 ± 1.1 mV ($n = 13$) in the control group (Fig. 2*B*,*C*, left). In the presence of the voltage-gated K^+ channel blockers (extracellular 20 mM TEA, and intracellular 135 mM Cs^+ plus 1 mM 4-AP), the noninactivating outward currents were smaller than those of the control group (Fig. 2*A* right, *B*,*C*). The reversal potential of the outward current in the presence of the voltage-gated K^+ channel blockers was −77.4 ± 1.6 mV ($n = 13$, Fig. 2*B*,*C*, left). We analyzed noninactivating outward currents using the area under the *I–V* curve (AUC), which showed that the voltage-gated K^+ channel blockers significantly reduced noninactivating outward currents (Fig. 2*B*,*C*, right panels). However noninactivating outward currents remain at high amplitudes in the presence of the voltage-gated potassium channel blockers (Fig. 2*B*,*C*).

Strong transient inward currents were detected at the NRs of lumbar spinal ventral nerves in response to depolarizing voltage steps. We tested effects of TTX on the transient inward currents evoked by depolarizing voltage steps at NRs of lumbar spinal ventral nerves. The transient inward currents were completely blocked by 500 nM TTX, suggesting that they were mediated by TTX-sensitive voltage-gated Na^+ channels (Fig. 3*A*). We isolated TTX-sensitive inward currents by subtracting total currents in the presence of TTX from the total currents in the absence of TTX (Fig. 3*B*). The *I–V* curve of the isolated transient inward currents were consistent with the currents mediated by TTX-sensitive voltage-gated Na^+ channels ($n = 5$, Fig. 3*C*). It should be noted that the *I–V* curve of the TTX-sensitive inward currents was distorted in the voltage for evoking the peak inward currents and the reversal potential. This was most likely because of a poor space-clamp for the large transient inward currents at the NRs.

Role of voltage-gated K^+ channels in intrinsic electrophysiological properties at the NRs of lumbar spinal ventral nerves

We determined electrophysiological properties of membranes and APs at the NRs of lumbar spinal ventral nerves. To investigate the role of voltage-gated K^+ channels in intrinsic electrophysiological properties at the NR, we examined effects of voltage-gated K^+ channel blockers on intrinsic electrophysiological properties at the NRs. RMP at the NRs was −85.0 ± 1.0 mV ($n = 12$, Fig. 4*A*,*B*) under the condition in the absence of voltage-gated K^+ channel blockers (control), and became significantly less negative at −76.2 ± 1.8 mV ($n = 13$, $p < 0.001$, Fig. 4*B*) in the presence of voltage-gated K^+ channel blockers 20 mM TEA in bath solution and 135 mM Cs^+ plus 1 mM 4-AP in recording electrode internal solution. The injection of depolarizing step currents resulted in nodal membrane depolarization and AP firing at the NRs once membrane depolarization reached AP threshold (Fig. 4*A*). AP threshold was −58.9 ± 1.5 mV ($n = 12$) in the control group, and significantly less negative at −52.2 ± 1.6 mV ($n = 13$) in the presence of the aforementioned voltage-gated K^+ channel blockers (Fig. 4*C*, $p < 0.05$). AP width was 0.9 ± 0.04 ms

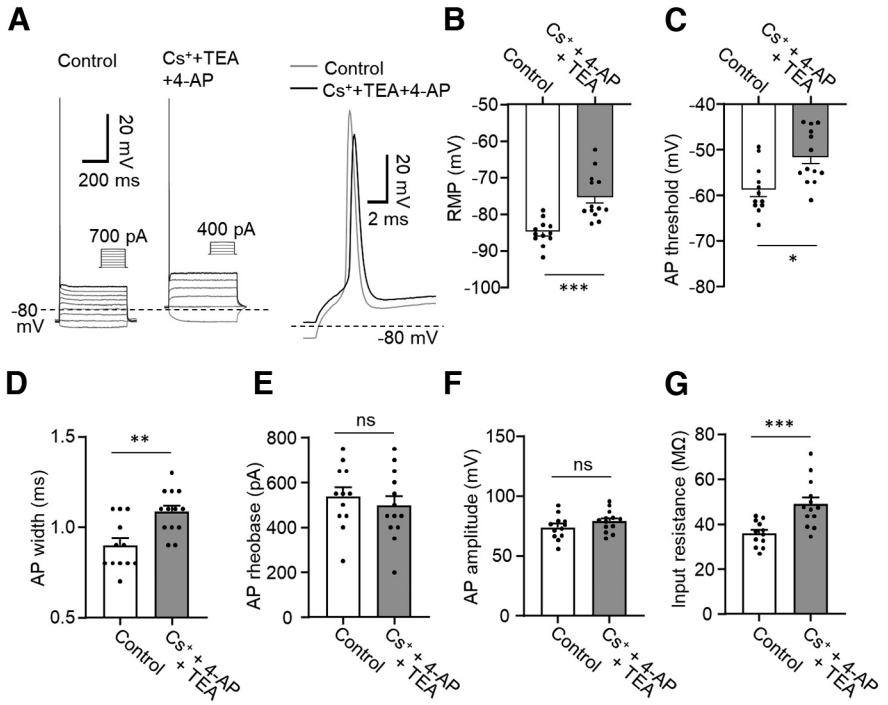

Figure 4. Effects of voltage-gated K^+ channel blockers on electrophysiological properties at the NR of lumbar spinal ventral nerves. ***A***, Sample traces represent APs recorded at an NR in the absence (control, left) and presence of the voltage-gated K^+ channel blockers Cs^+ + 4-AP + TEA (middle). Recordings were performed under the whole-cell current-clamp configuration, and step currents were injected into the NR through the recording electrode. Right, Overlay APs in the control (gray) and the presence of Cs^+ + 4-AP + TEA (black) at an expanded time scale. Voltage commands are shown under the sample current traces. ***B-G***, Bar graph represents the absence (control, open bars, $n = 12$) and presence of Cs^+ + 4-AP + TEA (gray bars, $n = 13$), nodal RMPs, (***B***), AP threshold (***C***), AP width (***D***), AP rheobase (***E***), AP amplitude (***F***), and membrane input resistance (***G***). In experiments with voltage-gated K^+ channel blockers, 135 mM Cs^+ plus 1 mM 4-AP were applied intracellularly, and 20 mM TEA was applied extracellularly. Data are mean ± SEM. ***$p < 0.001$ (Student's t test). ns, $p \geq 0.05$.

($n = 12$) in the control group, and significantly prolonged to 1.1 ± 0.03 ms ($n = 13$) in the presence of the voltage-gated K^+ channel blockers (Fig. 4*D*, $p < 0.01$). AP rheobase was 537.5 ± 40.4 pA ($n = 12$) in the control group, and 496.1 ± 42.2 pA ($n = 13$) in the presence of the voltage-gated K^+ channel blockers, and was not significantly different (Fig. 4*E*). AP amplitude was 68.2 ± 6.5 mV ($n = 12$) in the control group and 79.1 ± 2.5 mV ($n = 13$) in the presence of the voltage-gated K^+ channel blockers, and was not significantly different (Fig. 4*F*). Input resistance, measured under the voltage-clamp configuration following a −10 mV testing pulse from membrane holding voltage at −72 mV, was 35.8 ± 1.6 MΩ ($n = 12$) in the control group, and significantly increased to 49.0 ± 2.9 MΩ ($n = 13$) in the presence of the voltage-gated K^+ channel blockers (Fig. 4*G*, $p < 0.001$). Collectively, the results revealed roles of voltage-gated K^+ channels in the intrinsic electrophysiological properties of the NRs of lumbar spinal ventral nerves.

Role of voltage-gated K^+ channels in saltatory conduction at the NRs of lumbar spinal ventral nerves

To investigate the role of voltage-gated K^+ channels in saltatory conduction at the NRs, we determined whether block of voltage-gated K^+ channels affect saltatory conduction along lumbar spinal ventral nerves. In this set of experiments, electrical stimulation was applied to a distal site of lumbar spinal ventral nerves to orthodromically evoke APs, and APs were recorded at the NRs ~15 mm away from the stimulation site (Fig. 5*A*,*B*). We examined effects by TEA and 4-AP plus Cs^+ on AP propagation to the NRs at the recording sites. AP CV was 26.9 ± 2.2 m/s ($n = 7$) and 23.4 ± 2.3 m/s ($n = 6$) in the absence and presence of the voltage-gated K^+ channel blockers, respectively, and was not significantly different (Fig. 5*C*). We determined effects of the voltage-gated K^+ channel blockers on AP success rate at the NRs. In this set of experiments, APs were elicited at distal sites of lumbar spinal ventral nerves by train stimulation for 20 s at the frequencies of 1, 10, 50, 100, 200, 500, and 1000 Hz, and APs were recorded at the NRs. In the control group, AP success rate was 100% for stimulation frequencies from 1 to 100 Hz, and 73.0 ± 7.2% ($n = 6$) at train stimulation frequency of 200 Hz, 19.9 ± 2.3% ($n = 6$) at train stimulation frequency of 500 Hz and 3.5 ± 1.9% ($n = 6$) at train stimulation frequency of 1000 Hz (Fig. 5*D*,*E*). In the presence of TEA and 4-AP plus Cs^+, AP success rate reduced to 66.2 ± 17.8% ($n = 6$) at stimulation frequencies of 100 Hz, 22.5 ± 10.9% ($n = 6$) at train stimulation frequency of 200 Hz, 3.8 ± 2.7% ($n = 6$) at train stimulation frequency of 500 Hz, and 0.1 ± 0.1% ($n = 6$) at train stimulation frequency of 1000 Hz (Fig. 5*D*,*E*). Thus, the curve of AP success rate at different train stimulation frequencies showed left shift in the presence of the voltage-gated K^+ channel blockers (Fig. 5*E*). We used the frequency at which AP success rate was 50% (FS_{50}) to quantitatively describe the effect of voltage-gated K^+ channel blockers on the success rate of APs (Fig. 5*E*,*F*). FS_{50} was 302.2 ± 25.1 Hz ($n = 6$) in the control group, and significantly reduced to 156.3 ± 32.8 Hz ($n = 6$) in the presence of the voltage-gated K^+ channel blockers (Fig. 5*E*,*F*, $p < 0.01$). Together, the results suggest that voltage-gated K^+ channels play a regulatory role in the saltatory conduction at the NRs of lumbar spinal ventral nerves.

K2P-mediated K^+ currents at the NRs of lumbar spinal ventral nerves

Voltage-gated K^+ channel blockers only inhibited a small fraction of noninactivating outward currents at the NRs (Fig. 2), suggesting that most of the noninactivating outward currents may be mediated by leak K^+ or K2P channels. To directly investigate K2P-medaited currents at the NRs, we determined inhibitory effects on noninactivating outward currents at the NRs by compounds, which were previously shown to inhibit K2P channels (Enyedi and Czirjak, 2010). The compounds being tested included mibefradil (10 μM), Ba^{2+} (5 mM), spadin (1 μM), RR (200 μM), amlodipine (100 μM), NF (50 and 250 μM), Gd^{3+} (50 μM), chlopromazine (100 μM), diltiazem (1 mM), and bupivacaine (3 mM). Figure 6*A*–*C* shows inhibitory effects on noninactivating outward currents at the NRs of lumbar spinal ventral nerves by 50 and 250 μM NF ($n = 5$). The noninactivating outward currents were dose-dependently inhibited by 50 and 250 μM NF. Measured by the AUC, the noninactivating outward currents were inhibited by 27% by 50 μM NF ($n = 5$)

and 45% by 250 μM NF ($n = 5$; Fig. 6*C*). In addition to the inhibition of the noninactivating outward currents, it was noted that NF at 50 and 250 μM also inhibited the transient inward currents at the NRs (Fig. 6*A*). Bupivacaine, a voltage-gated Na^+ channel blocker, also showed strong inhibitory effects on the noninactivating outward currents at the NRs. Measured by the AUC, the noninactivating outward currents were inhibited by 60% by 3 mM bupivacaine ($n = 4$, Fig. 6*F*). In addition to the inhibition of the noninactivating outward currents, the transient inward currents at the NRs were also blocked by 3 mM bupivacaine (Fig. 6*D*). Figure 6*G* shows the summary data of the inhibitory effects of 11 compounds tested on noninactivating outward currents, and data represent changes of the AUCs (in reference to control) following the treatment of nerve preparations with each testing compound. While the 11 testing compounds blocked noninactivating outward currents at the NRs in different degrees (Fig. 6*G*), most of them also inhibited voltage-activated transient inward currents, which were mediated by TTX-sensitive voltage-gated Na^+ channels (Fig. 6*H*). For example, both NF at 250 μM and bupivacaine at 3 mM c>ompletely blocked the transient inward currents (Fig. 6*A*,*D*,*H*). Among these compounds, Ba^{2+} (5 mM), spadin (1 μM), and RR (200 μM) each inhibited noninactivating outward currents but had no significant effects on the transient inward currents (Fig. 6*G*,*H*). Noninactivating outward currents become 79.5 ± 3.0% ($n = 8$, $p < 0.001$), 75.6 ± 3.8% ($n = 10$, $p < 0.001$), and 74.2 ± 2.4% ($n = 7$, $p < 0.001$) in the presence of 5 mM Ba^{2+}, 1 μM spadin, and 200 μM RR, respectively (Fig. 6*G*). Thus, while many K2P channel blockers inhibited the noninactivating outward currents at the NRs of lumbar spinal ventral nerves, only a few of them appear to be suitable for exploring functions of K2P channels at the NRs.

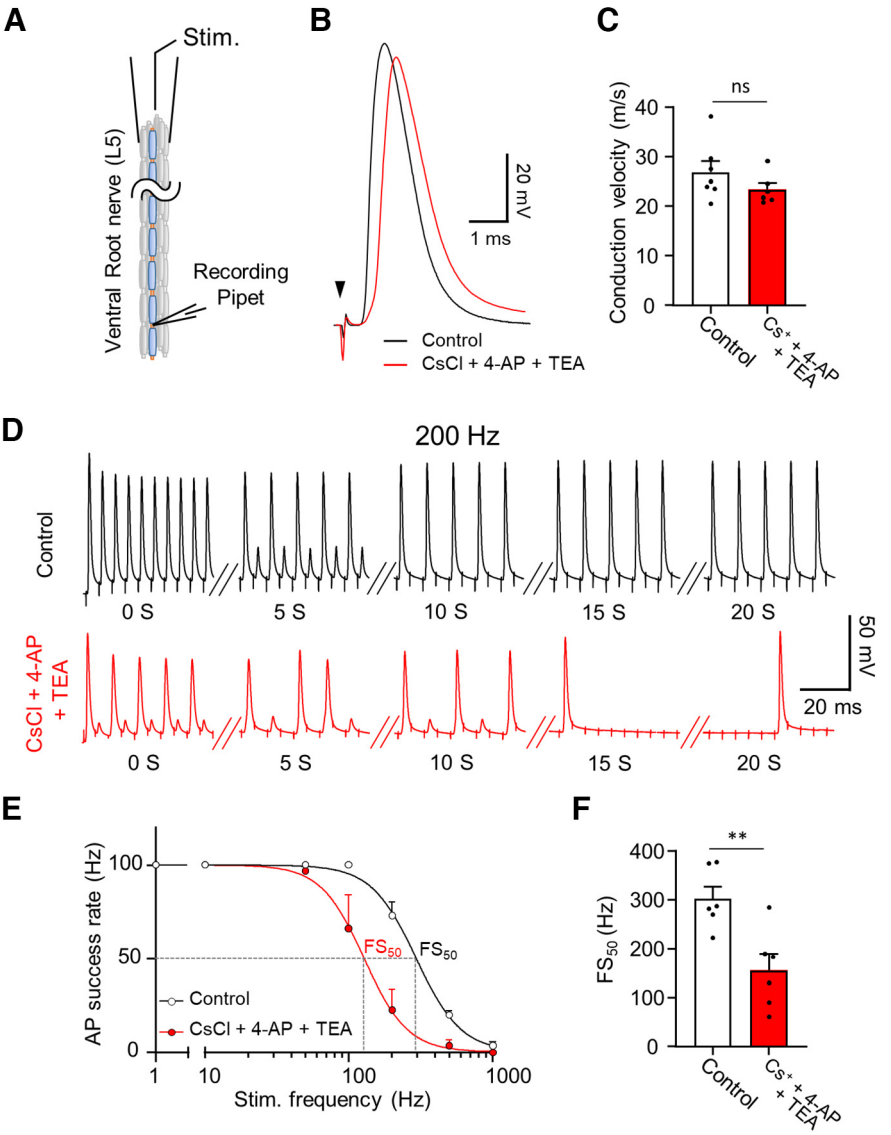

Figure 5. Effects of voltage-gated K^+ channel blockers on saltatory conduction through NR of lumbar spinal ventral nerves. ***A***, Experimental setting for recording action potentials through NRs of lumbar spinal ventral nerves. ***B***, Two overlay sample traces represent APs recorded from an NR following electrical stimulation applied to a distal site. The recordings were performed in the absence (control, black) and presence of Cs^+ + 4-AP + TEA (red). Arrow indicates stimulation artifact. ***C***, Summary data of AP CV determined from recordings shown in ***A***, ***B*** in control ($n = 7$) and the presence of Cs^+ + 4-AP + TEA ($n = 6$). ***D***, Two sets of sample trances represent APs recorded at an NR following a train of electrical stimulation at 200 Hz in control (top) and the presence of Cs^+ + 4-AP + TEA (bottom). Stimulation was applied for a period of 20 s. Only a short period of APs at initial time point (0 s), 5, 10, 15, and 20 s time point are presented to illustrate changes of AP success rates over the time period of 20 s. ***E***, AP success rates at NRs with distal stimulation at frequency of 1, 10, 100, 200, 500, and 1000 Hz ($n = 6$). Dashed lines indicate the frequency at which AP conduction success rates fall to 50% (FS_{50}). Recording duration at each frequency was 20 s. ***F***, Bar graphs represent summary data of FS_{50} in control ($n = 6$) and the presence of Cs^+ + 4-AP + TEA ($n = 6$). In experiments with voltage-gated K^+ channel blockers, 135 mM Cs^+ plus 1 mM 4-AP were applied intracellularly, and 20 mM TEA was applied extracellularly. Data are mean ± SEM. *$p < 0.05$; **$p < 0.01$; Student's *t* test. ns, $p \geq 0.05$.

Role of K2P channels in intrinsic electrophysiological properties at the NRs of lumbar spinal ventral nerves

To investigate the role of K2P channels in intrinsic electrophysiological properties at the NRs of lumbar spinal ventral nerves, we examined effects of RR (200 μM), Ba^{2+} (5 mM), and spadin (1 μM) on the membrane and AP properties at the NRs of lumbar spinal ventral nerves. These three compounds were tested because they inhibited noninactivating outward currents but did not have significant effects of the voltage-gated Na^+ currents at the NRs (Fig. 6*G*,*H*). Experiments were performed under the current-clamp configuration in the absence (control) and presence of RR (200 μM), Ba^{2+} (5 mM), or spadin (1 μM). RMP was −89.5 ± 1.8 mV ($n = 7$) in the control group, and depolarized to −84.2 ± 2.3 mV ($n = 7$, $p = 0.05$) in the presence of 200 μM RR (Fig. 7*A*). AP threshold was −60.1 ± 1.0 mV ($n = 7$) in the control group, and significantly increased to −45.3 ± 1.9 mV ($n = 7$) in the presence of RR (Fig. 7*B*, $p < 0.01$). AP width was 1.1 ± 0.03 ms ($n = 7$) in the control group, and significantly prolonged to 1.4 ± 0.09 ms ($n = 7$) in the presence RR (Fig. 7*C*, $p < 0.01$). AP amplitude was 106.2 ± 2.3 mV ($n = 7$) in the control

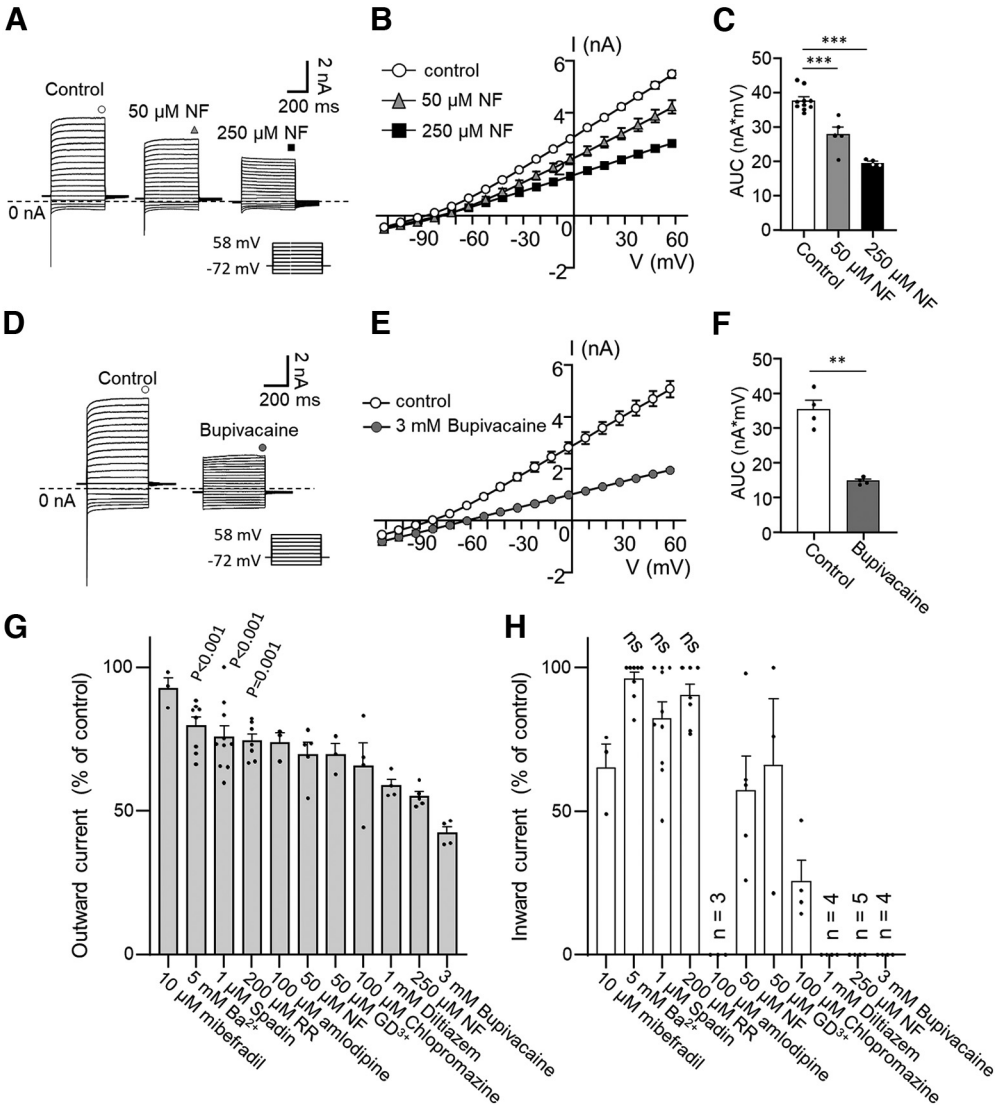

Figure 6. Effects of K2P channel blockers on noninactivating outward and transient inward currents at the NR of lumbar spinal ventral nerves. ***A***, Sample traces represent ionic currents recorded at an NR following voltage steps in the absence (control, left), presence of 50 μM (middle), and presence of 250 μM (right) of NF. ***B***, ***C***, *I–V* curves (***B***) and AUC (***C***) of noninactivation currents following voltage steps in control (circles in ***B*** and open bar in ***C***, $n = 10$), the presence of 50 μM (triangles in ***B*** and gray bar in ***C***, $n = 5$), and the presence of 250 μM (squares in ***B*** or black bar in ***C***, $n = 5$) NF. ***D***, Sample traces represent ionic currents recorded at an NR following voltage steps in the absence (control, left) and presence of 3 mM bupivacaine (right). ***E***, ***F***, *I–V* curves (***E***) and AUC (***F***) of noninactivation currents following voltage steps in control (open circles in ***E*** and open bar in ***F***, $n = 4$) and the presence of 3 mM bupivacaine (filled circle in ***E*** and or gray bar in ***F***, $n = 4$). ***G***, Pharmacological profile of noninactivating outward currents recorded at the NRs with 11 compounds known to block K2P channels. ***H***, Pharmacological profile of transient inward currents tested with the 11 compounds listed in ***G***. Statistical analyses were only applied to the testing groups of Ba^{2+} (5 mM, $n = 8$), spadin (1 μM, $n = 10$), and RR (200 μM, $n = 7$) since these compounds did not have inhibitory effects on the transient inward currents. Data are mean ± SEM. *$p < 0.05$; **$p < 0.01$; one-way ANOVA with Tukey *post hoc* test or Student's *t* test. ns, $p \geq 0.05$.

group, and significantly increased to 112.8 ± 1.4 mV ($n = 7$) in the presence of RR (Fig. 7*D*, $p < 0.05$). AP rheobase was 428.6 ± 47.4 pA ($n = 7$) in the control group, and significantly increased to 628.8 ± 55.5 pA ($n = 7$) in the presence of RR (Fig. 7*E*, $p < 0.01$). Input resistance was 44.1 ± 4.0 MΩ ($n = 7$) in the control group, and significantly increased to 52.1 ± 3.8 MΩ ($n = 7$) in the presence of RR (Fig. 7*F*, $p < 0.01$). We next investigated effects of Ba^{2+} on intrinsic electrophysiological properties of membranes and APs at the NRs. RMP was −83.6 ± 1.4 mV ($n = 8$) in the control group, and significantly depolarized to −78.2 ± mV ($n = 8$) in the presence of 5 mM Ba^{2+} (Fig. 7*G*, $p < 0.05$). AP threshold was −59.9 ± 2.1 mV ($n = 8$) in the control group, and significantly depolarized to −51.0 ± 0.6 mV ($n = 8$) in the presence of the Ba^{2+} (Fig. 7*H*, $p < 0.01$). AP width was 1.0 ± 0.03 ms ($n = 8$) in the control group, and significantly prolonged to 1.1 ± 0.05 ms ($n = 8$) in the presence of Ba^{2+} (Fig. 7*I*, $p < 0.01$). AP amplitude was 83.1 ± 4.8 mV ($n = 8$) in the control group and 85.4 ± 6.1 mV ($n = 8$) in the presence of Ba^{2+}, and was not significantly different (Fig. 7*J*). AP rheobase was 443.8 ± 67.8 pA ($n = 8$) in the control group, and significantly increased to 550.0 ± 59.8 pA ($n = 8$) in the presence of Ba^{2+} (Fig. 7*K*, $p < 0.05$). Input resistance was 43.1 ± 2.0 MΩ ($n = 8$) in the control group, and significantly increased to 63.2 ± 5.4 MΩ ($n = 8$) in the presence of Ba^{2+} (Fig. 7*L*, $p < 0.01$). Finally, we determined effects of spadin on intrinsic electrophysiological properties at the NRs. RMP was −85.3 ± 0.8 mV ($n = 10$) in the control group, and depolarized to −78.8 ± 2.9 mV ($n = 10$, $p = 0.05$, Fig. 7*M*) in the presence of spadin. AP threshold was −61.8 ± 1.3 mV (n= 10) in the control group, and became −55.1 ± 4.0 mV ($n = 10$) in the presence of the spadin ($p = 0.08$, Fig. 7*N*). AP width was 1.1 ± 0.09 ms ($n = 10$) in the control

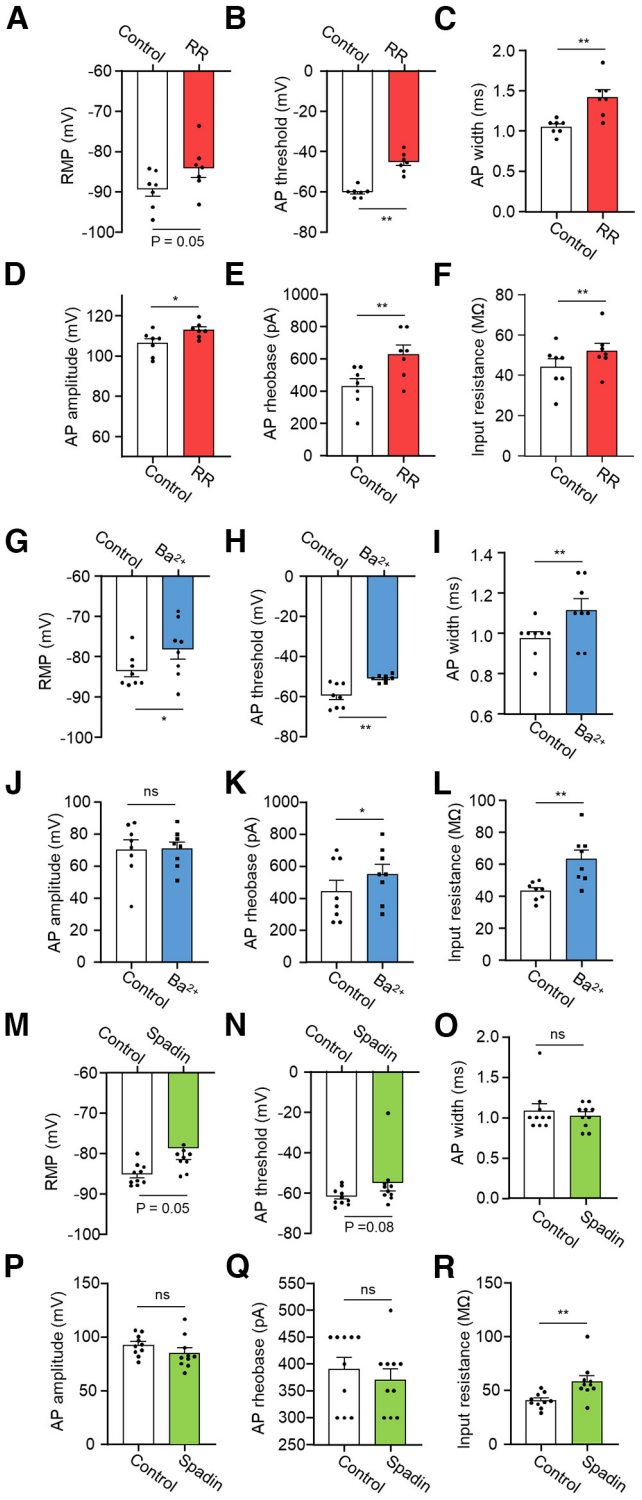

Figure 7. Effects of inhibiting K2P channels on electrophysiological properties at the NR of lumbar spinal ventral nerves. ***A-F***, Effects of RR on nodal RMP (***A***), AP threshold (***B***), AP width (***C***), AP amplitude (***D***), AP rheobase (***E***), and input resistance (***F***). The electrophysiological properties were determined in the absence (control, open bars) and presence of 200 μM RR ($n = 7$, red bars). ***G-L***, Effects of Ba^{2+} on nodal RMP (***G***), AP threshold (***H***), AP width (***I***), AP amplitude (***J***), AP rheobase (***K***), and input resistance (***L***). The electrophysiological properties were determined in the absence (control, open bars) and presence of 5 mM Ba^{2+} ($n = 8$, blue bars). ***M-R***, Effects of spadin on nodal RMP (***M***), AP threshold (***N***), AP width (***O***), AP amplitude (***P***), AP rheobase (***Q***), and input resistance (***R***). The electrophysiological properties were determined in the absence (control, open bars) and presence of 10 μM spadin ($n = 10$, green bars). Data are mean ± SEM. *$p < 0.05$; **$p < 0.01$; Student's *t* test. ns, $p \geq 0.05$.

group, and 1.0 ± 0.05 ms ($n = 10$) in the presence of spadin, and was not significantly different (Fig. 7*O*). AP amplitudes were 92.4 ± 3.1 mV ($n = 10$) in the control group and 84.8 ± 4.7 mV ($n = 10$) in the presence of spadin, and was not significantly different (Fig. 7*P*). AP rheobase was 390.0 ± 22.1 pA ($n = 10$) in the control group, and 370.0 ± 20.0 pA ($n = 10$) in the presence of spadin, and was not significantly different (Fig. 7*Q*). Input resistance was 40.6 ± 2.2 MΩ ($n = 10$) in the control group, and significantly increased to 58.3 ± 5.3 MΩ ($n = 10$) in the presence of spadin (Fig. 7*R*, $p < 0.01$). Collectively, the results demonstrate significant roles of K2P channels in the intrinsic electrophysiological properties of the NRs of lumbar spinal ventral nerves.

Role of K2P channels in saltatory conduction at the NRs of lumbar spinal ventral nerves

To determine the role of K2P channels in saltatory conduction at the NRs, we investigated whether K2P channel blockers affect saltatory conduction along lumbar spinal ventral nerves. In this set of experiments, electrical stimulation was applied to a distal site of lumbar spinal ventral nerves to evoke APs, and APs were recorded at the NRs ~15 mm away from the stimulation site. We examined effects of RR (200 μM) on the propagation of APs to the recording sites. AP CV was 37.8 ± 2.1 m/s ($n = 7$) in the absence of RR and significantly decreased to 30.7 ± 2.6 m/s ($n = 7$) in the presence of RR (Fig. 8*A*, $p < 0.01$). We determined effects of RR on AP success rates at the NRs in lumbar spinal ventral nerves. In this set of experiments, APs were elicited at distal sites of lumbar spinal ventral nerves by train stimulation for 20 s at the frequencies of 1, 10, 50, 100, 200, 500, and 1000 Hz, and APs were recorded at the NRs. In the control group, AP success rate was 100% for stimulation frequencies from 1 to 100 Hz, 90.2 ± 0.007% ($n = 7$) at train stimulation frequency of 200 Hz, 32.5 ± 5.0% ($n = 7$) at train stimulation frequency of 500 Hz, and 9.1 ± 3.5% ($n = 7$) at train stimulation frequency of 1000 Hz (Fig. 8*B*). In the presence of RR, AP success rate was 100% for stimulation frequencies from 1 to 100 Hz, and reduced to 65.4 ± 6.3% ($n = 7$) at train stimulation frequency of 200 Hz, 19.6 ± 3.5% ($n = 7$) at train stimulation frequency of 500 Hz, and 5.4 ± 1.9% ($n = 7$) at train stimulation frequency of 1000 Hz (Fig. 8*B*). The curve of AP success rate at different train stimulation frequency showed left shift in the presence of RR (Fig. 8*B*). We used the frequency at which AP success rate was 50% (FS_{50}) to quantitatively describe the effects of K2P channel blockers on the success rates of APs evoked by train stimuli (Fig. 8*C*). FS_{50} was 418.5 ± 37.8 Hz ($n = 7$) in the control group, and significantly reduced to 277.9 ± 27.0 Hz ($n = 7$) in the presence of RR (Fig. 8*C*, $p < 0.01$). We next determined effects on AP CV and APs success rate by Ba^{2+} and spadin. AP CV was 34.2 ± 2.2 m/s ($n = 7$) in the control group and significantly reduced to 28.5 ± 1.3 m/s in the presence 5 mM Ba^{2+} ($n = 7$, $p < 0.01$, Fig. 8*D*). AP CV was 35.3 ± 4.0 m/s ($n = 7$) in the control group and significantly reduced to 33.9 ± 4.3 m/s ($n = 7$) in the presence of 1 μM spadin (Fig. 8*G*, $p < 0.01$). However, both Ba^{2+} and spadin did not significantly affect AP success rates (Fig. 8*E*,*F*,*H*,*I*). Together, the results suggest that K2P channels play a role in the saltatory conduction at the NRs of lumbar spinal ventral nerves.

Effects of cooling temperatures on ionic currents at the NRs of lumbar spinal ventral nerves

K2P channels can be inhibited by cooling temperatures (Kanda et al., 2019, 2021b). We tested effects of cooling temperatures on the noninactivating outward currents at the NRs of lumbar ventral nerves. Noninactivating outward currents were strong and

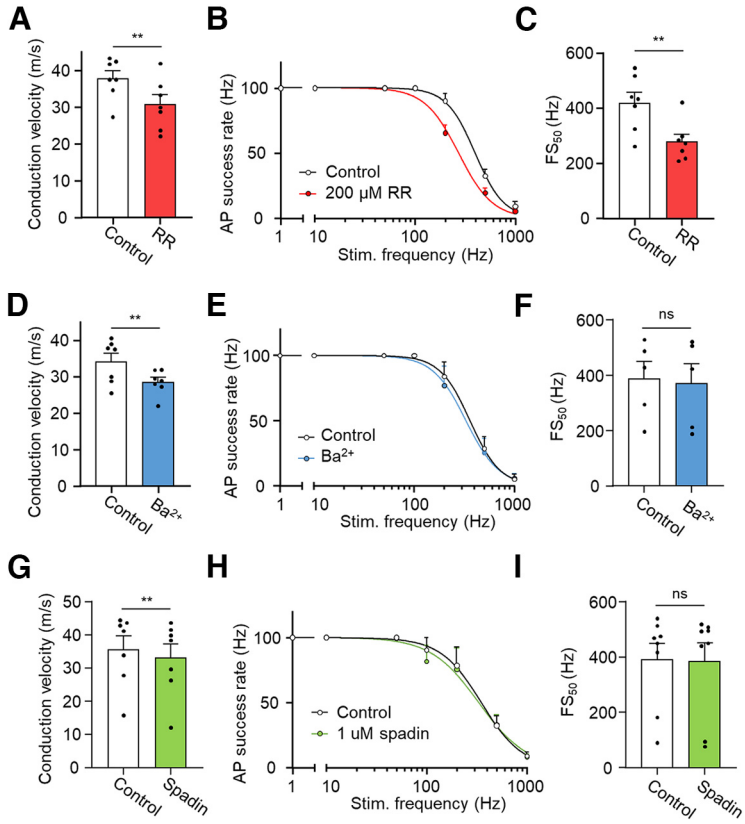

Figure 8. Effects of inhibiting K2P channels on saltatory conduction at the NR of lumbar spinal ventral nerves. ***A***, Summary data of AP CV determined in the absence (control) and presence of 200 μM RR ($n = 7$). ***B***, AP success rates at NRs with distal stimulation at frequency of 1, 10, 100, 200, 500, and 1000 Hz ($n = 7$) determined in control and the presence of 200 μM RR ($n = 7$). Recording duration at each frequency was 20 s. ***C***, Bar graphs represent summary data of FS_{50} ($n = 7$) in control and the presence of 200 μM RR ($n = 7$). ***D***, Summary data of AP CV determined in the absence (control) and presence of 5 mM Ba^{2+} ($n = 7$). ***E***, AP success rates at NRs with distal stimulation at frequency of 1, 10, 100, 200, 500, and 1000 Hz ($n = 5$) determined in control and the presence of 5 mM Ba^{2+} ($n = 5$). Recording duration at each frequency was 20 s. ***F***, Bar graphs represent summary data of FS_{50} ($n = 5$) in control and the presence of 5 mM Ba^{2+} ($n = 5$). ***G***, Summary data of AP CV determined in the absence (control) and presence of 1 μM spadin ($n = 7$). ***H***, AP success rates at NRs with distal stimulation at frequency of 1, 10, 100, 200, 500, and 1000 Hz ($n = 7$) determined in control and in the presence of 1 μM spadin ($n = 7$). Recording duration at each frequency was 20 s. ***I***, Bar graphs represent summary data of FS_{50} ($n = 7$) in control and the presence of 1 μM spadin ($n = 7$). In all experiments, whole-cell current-clamp recordings were performed at NRs and APs were evoked by electrical stimulation from distal sites of nerve bundles. Data represent mean ± SEM. *$p < 0.05$; **$p < 0.01$; Student's *t* test. ns, $p \geq 0.05$.

had large amplitudes at 35°C and progressively reduced when temperatures were reduced to 24°C and 15°C (Fig. 9*A*,*B*). The *I–V* curves of the noninactivating outward currents had reversal potentials of −83.0 ± 1.2 mV ($n = 9$) at 35°C, −85.1 ± 1.3 mV ($n = 9$) at 24°C, and −80.1 ± 1.7 mV ($n = 9$) at 15°C, and were significantly different between 24°C and 15°C ($p < 0.05$). Expressed as AUC, the noninactivating outward currents were 46.9 ± 2.8 nA*mV ($n = 9$) at 35°C, significantly reduced to 37.3 ± 2.0 nA*mV ($n = 9$, $p < 0.001$) at 24°C, and to 28.3 ± 1.9 nA*mV ($n = 9$, $p < 0.001$) at 15°C; the noninactivating outward currents were significantly lower at 24°C and 15°C compared with those at 35°C (Fig. 9*C*). The AUC of transient inward currents was 48.1 ± 6.3 nA*mV ($n = 9$) at 35°C, significantly reduced to 31.4 ± 3.7 nA*mV ($n = 9$, $p < 0.001$) at 24°C, and to 17.1 ± 2.3 nA*mV ($n = 9$, $p < 0.001$) at 15°C (Fig. 9*D*).

Effects of cooling temperatures on intrinsic electrophysiological properties of lumbar spinal ventral nerves

We determined effects of cooling temperatures on the membrane and AP properties at the NRs of lumbar spinal ventral nerves. Experiments were performed under the current-clamp configuration with bath solution at the temperatures of 35°C, 24°C, and 15°C (Fig. 10*A*). RMP was −83.3 ± 1.7 mV ($n = 9$) at 35°C, −85.7 ± 1.4 mV ($n = 9$) at 24°C, and −80.3 ± 2.1 mV ($n = 9$) at 15°C, and was significantly different between 24°C and 15°C (Fig. 10*B*, $p < 0.05$). AP width was 0.5 ± 0.03 ms ($n = 8$) at 35°C and significant prolonged to 1.0 ± 0.05 ms ($n = 8$, $p < 0.001$) at 24°C, and 1.9 ± 0.08 ms ($n = 8$, $p < 0.001$) at 15°C (Fig. 10*C*). AP amplitude was 74.3 ± 3.4 mV ($n = 8$) at 35°C, and significant increased to 88.8 ± 13.4 mV ($n = 8$, $p < 0.001$) at 24°C, and 88.6 ± 6.1 mV ($n = 8$, $p < 0.05$) at 15°C (Fig. 10*D*). AP threshold was −58.9 ± 2.0 mV ($n = 8$) at 35°C, −59.7 ± 2.0 mV ($n = 8$) at 24°C, and −54.8 ± 2.6 mV ($n = 8$) at 15°C, and was not significantly different (Fig. 10*E*). Time to threshold was 2.3 ± 0.1 ms ($n = 8$) at 35°C and significant increased to 5.1 ± 0.7 ms ($n = 8$, $p < 0.001$) at 24°C, and 5.8 ± 1.0 ms ($n = 8$, $p < 0.01$) at 15°C (Fig. 10*F*). AP rheobase was 718.8 ± 70.0 pA ($n = 8$) at 35°C, and significantly decreased to 512.5 ± 50.7 pA ($n = 8$, $p < 0.01$) at 24°C, and 418.8 ± 42.2 pA ($n = 8$, $p < 0.01$) at 15°C (Fig. 10*G*). Input resistance was 31.2 ± 2.5 MΩ ($n = 8$) at 35°C, and significant increased to 37.6 ± 2.9 MΩ ($n = 8$, $p < 0.01$) at 24°C, and 47.4 ± 4.5 MΩ ($n = 8$, $p < 0.001$) at 15°C (Fig. 10*H*).

Effects of cooling temperatures on saltatory conduction along lumbar spinal ventral nerves

We investigated effects of cooling temperatures on saltatory conduction of APs along lumbar spinal ventral nerves. In this set of experiments, electrical stimulation was applied to a distal site of lumbar spinal ventral nerves to evoke APs, and APs were recorded at the NRs ~15 mm away from the stimulation site (Fig. 11*A*). We determined CV of APs at 35°C, 24°C, and 15°C. AP CV was 41.9 ± 4.0 m/s ($n = 7$) at 35°C, significant decreased to 29.4 ± 1.1 m/s ($n = 7$, $p < 0.05$) at 24°C, and 18.3 ± 1.5 mV ($n = 7$, $p < 0.01$) at 15°C (Fig. 11*B*). We also examined effects of cooling temperatures on the properties of APs conducted to the recording sites. AP width was 0.4 ± 0.04 ms ($n = 7$) at 35°C, and significantly prolonged to 0.8 ± 0.04 ms ($n = 7$, $p < 0.001$) at 24°C, and 1.7 ± 0.06 ms ($n = 7$, $p < 0.001$) at 15°C (Fig. 11*C*). AP amplitude was 78.7 ± 3.5 mV ($n = 7$) at 35°C, 95.0 ± 3.7 mV ($n = 7$) at 24°C, and 83.7 ± 6.3 mV ($n = 7$) at 15°C, and was significantly different between 35°C and 24°C (Fig. 11*D*, $p < 0.01$).

We investigated effects of cooling temperatures on AP success rates at the NRs of lumbar spinal ventral nerves. In this set of experiments, APs were elicited at distal sites of lumbar spinal ventral nerves by train stimulation for 20 s at the frequencies of 1, 10, 50, 100, 200, 500, and 1000 Hz. APs were recorded at the NRs at 35°C, 24°C, and 15°C. Figure 12*A* shows sample traces of APs evoked by 200 Hz stimuli for 20 s at 35°C, 24°C, and 15°C. AP success rates were progressively reduced with decreasing temperatures from 35°C to 24°C and 15°C. At 35°C, AP success

rate was 100% for stimulation frequencies from 1 to 200 Hz, 39.0 ± 10.8% ($n = 6$) at train stimulation frequency of 500 Hz, and 9.6 ± 3.8% ($n = 6$) at train stimulation frequency of 1000 Hz (Fig. 12*B*). At 24°C, AP success rate was 100% for stimulation frequencies from 1 to 100 Hz, and reduced to 73.0 ± 7.2% at train stimulation frequency of 200 Hz, 19.9 ± 2.2% ($n = 6$) at train stimulation frequency of 500 Hz, and 3.5 ± 1.9% ($n = 6$) at train stimulation frequency of 1000 Hz (Fig. 12*B*). At 15°C, AP success rate was 100% for stimulation frequencies from 1 to 10 Hz, and reduced to 82.9 ± 10.4% ($n = 6$) at the train stimulation frequency of 50 Hz, 38.9 ± 8.0% ($n = 6$) at 100 Hz train stimulation, 15.5 ± 3.7% ($n = 6$) at 200 Hz train stimulation, 0.6 ± 0.4% ($n = 6$) at 500 Hz train stimulation, and 0.008 ± 0.002% ($n = 6$) at 1000 Hz train stimulation (Fig. 12*B*). Thus, the curve of AP success rate at different train stimulation frequency showed left shift at cooling temperatures (Fig. 12*B*). We used the frequency at which AP success rate was 50% (FS_{50}) to quantitatively describe the effects of temperatures on the success rates of APs evoked by train stimuli (Fig. 12*C*). FS_{50} was 497.5 ± 43.4 Hz ($n = 6$) at 35°C, significantly reduced to 302.2 ± 25.1 Hz ($n = 6$, $p < 0.01$) at 24°C, and 90.7 ± 12.1 Hz ($n = 6$, $p < 0.001$) at 15°C (Fig. 12*C*).

Discussion

In the present study, we have used the *ex vivo* lumbar spinal ventral nerve preparation and applied pressure-patch-clamp recordings to investigate K^+ channels and their roles in intrinsic electrophysiological properties and saltatory conduction at the NRs of lumbar spinal ventral nerves. We have characterized effects on the intrinsic electrophysiological properties and saltatory conduction at the NRs by voltage-gated K^+ channel blockers, K2P channel blockers, and cooling temperatures. To our knowledge, this is the first whole-cell patch-clamp recording study at the NRs of motor nerve fibers of mammals. We have demonstrated that NRs of lumbar spinal ventral nerves expressed a significant level of voltage-gated K^+ channels. However, K2P channels remain to be the principal K^+ channels at the NRs of these nerve fibers. We have shown that both K2P and voltage-gated K^+ channels play significant roles in intrinsic electrophysiological properties and saltatory conduction at NRs of lumbar spinal ventral nerves. Inhibition of voltage-gated K^+

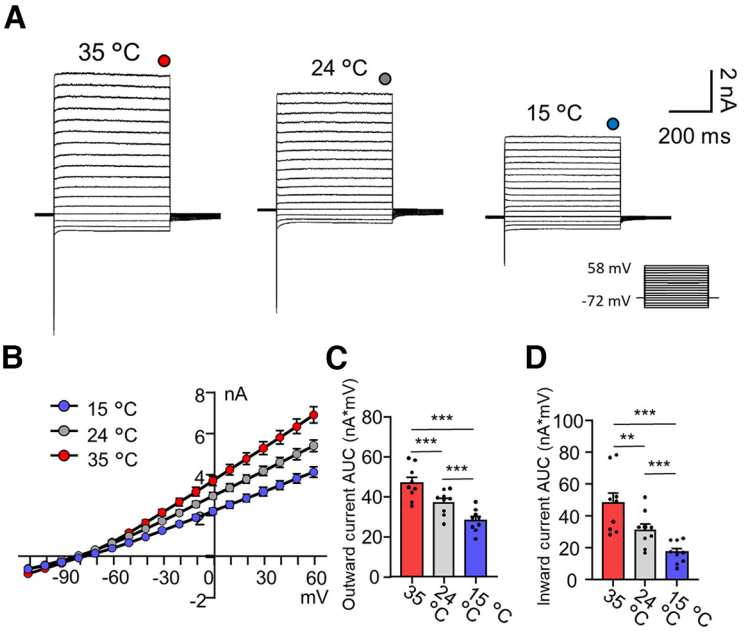

Figure 9. Effects of cooling temperatures on ionic currents at the NR of lumbar spinal ventral nerves. ***A***, Sample traces represent currents recorded at an NR following voltage steps at 35°C (left), 24°C (middle), and 15°C (right). Circles represent the places where the noninactivating outward currents are used to plot *I–V* relationship in ***B***. ***B***, *I–V* curves of noninactivating currents at 35°C (red circles, $n = 9$), 24°C (gray circles, $n = 9$), and 15°C (blue circles, $n = 9$). ***C***, AUC of the noninactivating currents at 35°C (red bar, $n = 9$), 24°C (white bar, $n = 9$), and 15°C (blue bar, $n = 9$). ***D***, AUC of the inward currents evoked by voltage steps at 35°C (red bar, $n = 9$), 24°C (white bar, $n = 9$), and 15°C (blue bar, $n = 9$). Data are mean ± SEM. $*p < 0.05$; $**p < 0.01$; one-way ANOVA with Tukey *post hoc* test.

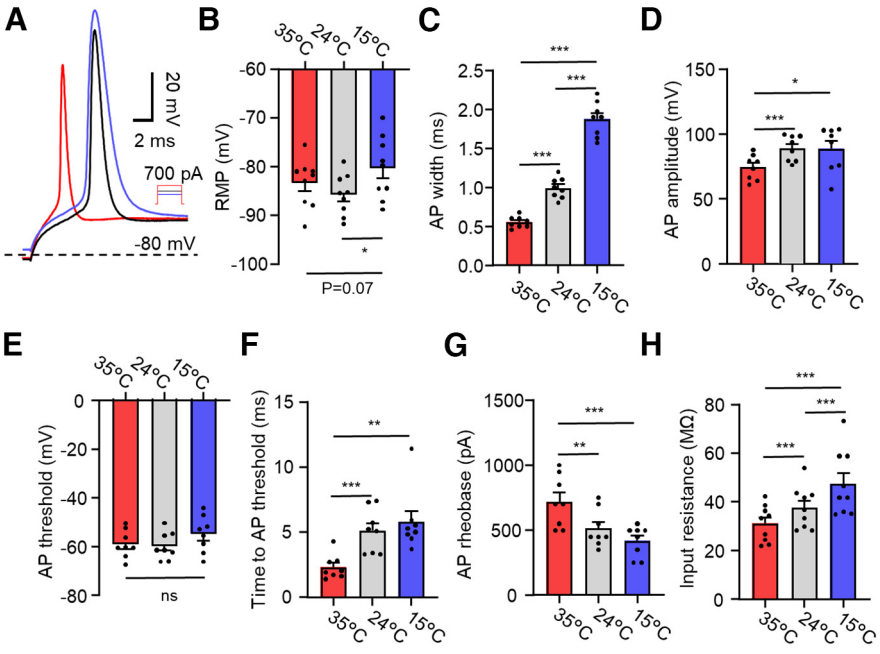

Figure 10. Effects of cooling temperatures on intrinsic electrophysiological properties of lumbar spinal ventral nerves. ***A***, Sample traces represent RMP and APs recorded at 35°C (red), 24°C (black), and 15°C (blue). Recordings were performed under the whole-cell current-clamp configuration, and step currents were injected into the NR through the recording electrode. ***B-H***, Bar graph represents recordings at NRs performed at 35°C (red bars, $n = 8$), 24°C (gray bars, $n = 8$), and 15°C (blue bars, $n = 8$) for nodal RMP (***B***), AP width (***C***), AP amplitude (***D***), AP threshold (***E***), time to AP threshold (***F***), AP rheobase (***G***), and membrane input resistance (***H***). Data are mean ± SEM. $*p < 0.05$; $**p < 0.01$; $***p < 0.001$; one-way ANOVA with Tukey *post hoc* test.

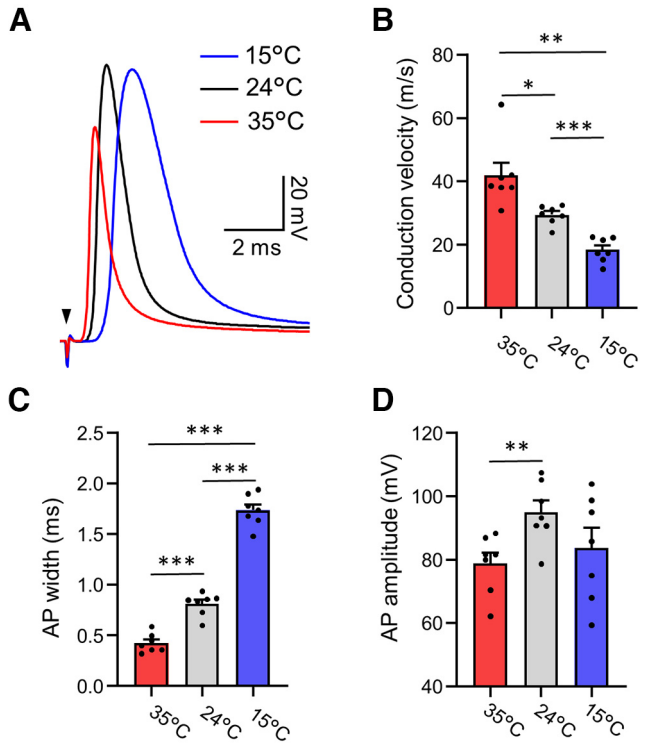

Figure 11. Effects of cooling temperatures on the velocity of saltatory conduction along lumbar spinal ventral nerves. ***A***, Three overlay sample traces show APs recorded from an NR following electrical stimulation applied to a distal site. The recordings were performed at 35°C (red), 24°C black), and 15°C (blue). Arrowhead indicates stimulation artifact. ***B***, Summary data of AP CV determined from recordings shown in ***A*** at 35°C (red bar, $n = 7$), 24°C (gray bar, $n = 7$), and 15°C (blue bar, $n = 7$). ***C***, ***D***, Summary data of widths and amplitudes of nodal APs ($n = 7$) evoked by electrical stimulation at distal locations. Data are mean ± SEM. $^*p < 0.05$; $^{**}p < 0.01$; $^{***}p < 0.001$; one-way ANOVA with Tukey *post hoc* test.

channels and K2P channels by their blockers or cooling temperatures significantly alters the intrinsic electrophysiological properties and saltatory conduction at the NRs of lumbar spinal ventral nerves.

Patch-clamp recordings at the NRs are technically challenging and have never been used previously at the NRs of motor nerve fibers of mammals. We applied pressure-patch-clamp recording technique that we recently developed (Kanda et al., 2019, 2021a,b) to investigate ion channels and their functions at the NRs of motor nerve fibers. In addition, we included AlexaFluor-555 in the recording electrode to label axons of recorded nerve fibers and visualize morphologic characteristics of the axons of these nerve fibers. The axons of lumbar spinal ventral nerves were morphologically similar to those of trigeminal Aβ-afferent somatosensory nerves shown in our previous study (Kanda et al., 2019). However, the diameter and length of NRs in the lumbar spinal ventral nerves were found to be greater than those of trigeminal Aβ-afferent nerves (Kanda et al., 2019). This size difference of the NRs may partially contribute to the differences in electrophysiological properties of NRs between motor nerves and somatosensory nerves.

At the NRs of rat lumbar spinal ventral nerves, we show that voltage-activated inward currents could be completely blocked by TTX, indicating these inward currents are mediated by TTX-sensitive voltage-gated Na^+ channels. These channels are most likely to be NaV1.6 channels since strong immunoreactivity of NaV1.6 has been shown to be clustered at the NRs (Caldwell et al., 2000; Waxman, 2006). We show that voltage-gated K^+ channels are present at a significant level at the NRs on lumbar spinal ventral nerves. This is evidenced by the significant inhibition of noninactivating outward currents by the voltage-gated K^+ channel blockers TEA and 4-AP plus Cs^+. Immunohistochemical studies have shown the presence of Kv7.2 immunoreactivity at the NRs of myelinated nerve fibers (Devaux et al., 2004). Thus, the noninactivating outward currents that are sensitive to voltage-gated K^+ channel blockers in the present study are most likely mediated by Kv7.2 channels. In addition to Kv7.2, immunoreactivity to Kv1.1 and Kv1.2 channels has been observed in paranodal regions of myelinated nerve fibers (Rhodes et al., 1997), raising a possibility that these voltage-gated K^+ channels may also mediate the noninactivating outward currents at the NRs. However, voltage-gated K^+ channels at paranodal regions are thought to be functionally silent in intact NRs (Chiu and Ritchie, 1980). Nevertheless, they are believed to contribute to the enhanced outward currents following nerve demyelination (Chiu and Ritchie, 1980, 1981). In the present study, noninactivating outward currents recorded at the NRs of motor nerve fibers remain to have high amplitudes in the presence of the voltage-gated K^+ channel blockers. This result suggests that voltage-gated K^+ channels are not the principal K^+ channels at the NRs of motor fibers. In the present study, NF, bupivacaine, and other K2P channels blockers (Maingret et al., 1999, 2000; Kim et al., 2001; Kang et al., 2005; Enyedi and Czirjak, 2010) significantly inhibited the noninactivating outward currents at the NRs of lumbar spinal ventral nerves, suggesting the noninactivating outward currents are largely mediated by K2P channels. Furthermore, the noninactivating outward currents at the NRs of the lumbar spinal ventral nerve fibers are highly temperature-sensitive and significantly inhibited at cooling temperatures, suggesting that the noninactivating outward currents are mediated by thermal K2P channels. This is consistent with somatosensory nerves which express thermal K2P channels TREK1 and TRAAK at their NRs. However, in somatosensory nerves, noninactivating outward currents are mostly, if not exclusively, mediated by thermal K2P channels, and the involvement of voltage-gated K^+ channels is negligible (Kanda et al., 2019).

We have demonstrated that voltage-gated K^+ channels play significant roles in intrinsic electrophysiological properties at the NRs of lumbar spinal ventral nerves, as is evidenced by the changes of intrinsic electrophysiological properties following the application of voltage-gated K^+ channel blockers. For example, RMP at the NRs becomes significantly depolarized and membrane input resistance significantly increased following the application of the voltage-gated K^+ channel inhibitors. These results suggest that voltage-gated K^+ channels, most likely Kv7.2 channels, are involved in passive membrane properties at the NRs. We show that voltage-gated K^+ channel blockers significantly prolonged AP width at the NRs, suggesting that these channels are partially involved in AP repolarization at the NRs of motor nerve fibers. In contrast to these effects on the intrinsic electrophysiological properties in motor nerve fibers, in our previous study, voltage-gated K^+ channel blockers did not significantly affect intrinsic electrophysiological properties of NRs at somatosensory Aβ-afferent nerves (Kanda et al., 2019).

We show that K2P channels also play significant roles in intrinsic electrophysiological properties at the NRs of motor nerve fibers, as is evidenced by the changes of the intrinsic electrophysiological properties following the application of K2P

channel blockers. In the present study, a number of compounds that are previously shown to be K2P channel blockers (Maingret et al., 1999, 2000; Kim et al., 2001; Kang et al., 2005; Enyedi and Czirjak, 2010) significantly inhibited noninactivating outward currents at the NRs of lumbar spinal ventral nerves. Among the 11 tested compounds, Ba^{2+}, RR, and spadin inhibited the outward currents without affecting voltage-activated inward currents at the NRs. Therefore, they appear to be suitable for studying the role of K2P channels in intrinsic electrophysiological properties and saltatory conduction at the NRs. However, it should be noted that RR has previously been found to inhibit mitochondrial Ca^{2+} uniporter and TRPV2 channels (Broekemeier et al., 1994; Shibasaki et al., 2010). We show that RR, Ba^{2+}, and spadin depolarized RMPs and increased input resistance, suggesting a potential role of K2P channels in passive membrane properties at the NRs of motor nerve fibers. This result is consistent with our previous study on the role of K2P channels at NRs of somatosensory nerves (Kanda et al., 2019, 2021b). AP width was prolonged by Ba^{2+} and RR, which may suggest that K2P channels play a role in AP repolarization at the NRs of motor nerve fibers. In somatosensory Aβ-afferent nerves, K2P channels at the NRs play a key role in AP repolarization since voltage-gated K^+ channels are functionally negligible (Kanda et al., 2019). We have observed that the inhibition of K2P channels and also voltage-gated K^+ channels decreased rather than increased nodal membrane excitability since AP threshold becomes higher (less negative). One possible reason for this effect is that the inhibition of these K^+ channels shifts RMP to a much less negative level, which leads to large steady-state inactivation of voltage-gated Na^+ channels and thereby resulting in the reduction of membrane excitability at the NRs.

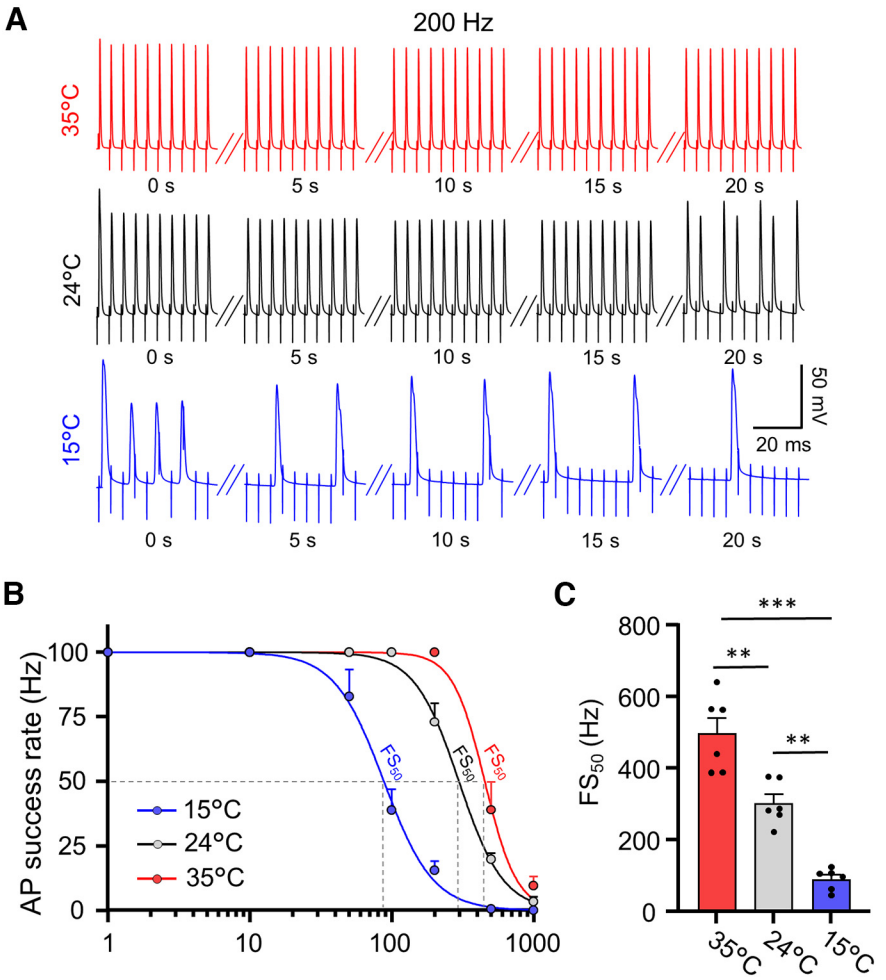

Figure 12. Effects of cooling temperatures on AP success rates at the NR of lumbar spinal ventral nerves. ***A***, Three sample traces represent APs recorded at an NR following a train of electrical stimulation at 200 Hz at 35°C (top), 24°C (middle), and 15°C (bottom). In each test, stimulation was applied at a distal site for a period of 20 s. ***B***, AP success rates at NRs with distal stimulation at frequency of 1, 10, 100, 200, 500, and 1000 Hz ($n = 6$). Dashed lines indicate the frequency at which AP conduction success rate fall to 50% (FS_{50}). Recording duration at each frequency was 20 s. ***C***, Bar graphs represent summary data of FS_{50} at 35°C (red, $n = 6$), 24°C (gray, $n = 6$), and 15°C (blue, $n = 6$). Data are mean ± SEM. $^*p < 0.05$; $^{**}p < 0.01$; $^{***}p < 0.001$; one-way ANOVA with Tukey *post hoc* test.

We have observed that cooling temperatures have profound effects on intrinsic electrophysiological properties at the NRs of motor nerve fibers. Some of these effects, for example, depolarizing RMP, increasing input resistance, reducing AP rheobase, and prolonging AP width are similar to the effects of K2P inhibitors. These results may suggest that the effects of cooling temperatures on intrinsic electrophysiological properties of NRs are at least partially mediated by the inhibition of K2P channels. These results are consistent with the strong immunoreactivity of thermal K2P channels at the NRs of different peripheral nerves, including motor nerve fibers (Brohawn et al., 2019; Kanda et al., 2019). We show that cooling temperatures increase AP amplitude at the NRs. The increase of AP amplitude at cooling temperatures has been previously reported in the giant axons of the squid (Hodgkin and Katz, 1949). At the NRs, thermal K2P channels could be inhibited by cooling temperatures to substantially increase nodal membrane input resistance, which would increase the efficiency of voltage-gated Na^+ channels for generating APs with greater amplitudes. In contrast, cooling temperatures reduce AP amplitude on the somas of somatosensory neurons (Zimmermann et al., 2007), which may be because of the reduction of voltage-gated Na^+ channel availability at cooling temperatures.

We have demonstrated that saltatory CV of the lumbar spinal ventral nerves is not significantly affected by voltage-gated K^+ channel blockers. However, voltage-gated K^+ channel blockers significantly reduced AP success rates at high-frequency stimulation. The lack of effect by voltage-gated K^+ channel blockers on saltatory CV in the present study is consistent with a previous study performed on rat sciatic nerves (Rasband et al., 1998). The significant reduction of AP success rates at high-frequency stimulation by voltage-gated K^+ channel blockers suggests that voltage-gated K^+ channels play a role in securing AP conduction at high frequency in motor nerve fibers. In contrast to voltage-gated K^+ channel, we show that K2P channels at NRs are involved in high-speed saltatory conduction as is evidenced by the reduction of saltatory CV by K2P channel blockers RR, Ba^{2+} and spadin. This result is consistent with our previous study on

the role of K2P channels in saltatory conduction on somatosensory Aβ-afferent nerves (Kanda et al., 2019). K2P channels at NRs maintained nodal membranes at a lower input resistance, which would shorten nodal membrane time constant. Based on studies with computational modeling, it has been suggested that the speed of membrane charge or membrane time constant for AP initiation at NRs may be a rate-limiting factor for saltatory CV (Castelfranco and Hartline, 2015, 2016). Biophysically, the speed of membrane charge is faster with smaller membrane capacitance and also with smaller membrane input resistance (Halter and Clark, 1993; Castelfranco and Hartline, 2016). In addition, the role of K2P channels in maintaining very negative RMPs and rapid AP repolarization may also be contributing factors for high-speed saltatory conduction. In the present study, we show AP success rates at high stimulation frequency were reduced by RR, suggesting K2P channels may be involved in securing high-frequency AP conduction in motor nerves. However, the lack of effects by Ba^{2+} and spadin on AP success rates raises a possibility that RR may have nonspecific effects on AP success rates. Alternatively, the lack of significant effect on AP success rates by Ba^{2+} and spadin could be because of their weak inhibition on K2P channels.

We have found that cooling temperatures not only reduced saltatory conduction speed but also decreased AP success rates at high-frequency stimulation. The effects of cooling temperatures are at least partially because of the inhibition of K2P channels and voltage-gated K^+ channels. The inhibition of K2P and voltage-gated K^+ channels could depolarize RMPs, which would promote steady-state inactivation of voltage-gated Na^+ channels to decrease their availability for APs (Zimmermann et al., 2007; Kanda et al., 2021a). The inhibition of K2P and voltage-gated K^+ channels by cooling temperatures slows AP repolarization and broadens AP width, which may also account for the effects of cooling temperatures on saltatory conduction as shown in the present study. Furthermore, cooling temperatures directly inhibit voltage-gated Na^+ channels and induce steady-state inactivation of voltage-gated Na^+ channels. These multiple factors may underlie the effects of cooling temperatures on saltatory conduction.

In conclusion, the findings in the present study provide ion channel bases for the intrinsic electrophysiological properties of nodal membranes and uncovered functions of voltage-gated K^+ channels and K2P channels in saltatory conduction on motor nerve fibers of rats. One physiological implication of this study is the effect of cooling temperatures on saltatory conductions as demonstrated in the present study. It would be interesting to know whether these K^+ channels are present at the NRs of human motor nerves and play similar roles as shown in the present study. Future studies on ion channels and their potential dysfunctions at the NRs of motor nerves may provide novel pathologic mechanisms in demyelination disorders and therapeutic implications.

References

Arancibia-Carcamo IL, Attwell D (2014) The node of Ranvier in CNS pathology. Acta Neuropathol 128:161–175.

Bean BP (2007) The action potential in mammalian central neurons. Nat Rev Neurosci 8:451–465.

Binah O, Palti Y (1981) Potassium channels in the nodal membrane of rat myelinated fibres. Nature 290:598–600.

Boullerne AI (2016) The history of myelin. Exp Neurol 283:431–445.

Broekemeier KM, Krebsbach RJ, Pfeiffer DR (1994) Inhibition of the mitochondrial Ca^{2+} uniporter by pure and impure ruthenium red. Mol Cell Biochem 139:33–40.

Brohawn SG, Wang W, Handler A, Campbell EB, Schwarz JR, MacKinnon R (2019) The mechanosensitive ion channel TRAAK is localized to the mammalian node of Ranvier. Elife 8:e50403.

Caldwell JH, Schaller KL, Lasher RS, Peles E, Levinson SR (2000) Sodium channel Na(v)1.6 is localized at nodes of Ranvier, dendrites, and synapses. Proc Natl Acad Sci USA 97:5616–5620.

Castelfranco AM, Hartline DK (2015) The evolution of vertebrate and invertebrate myelin: a theoretical computational study. J Comput Neurosci 38:521–538.

Castelfranco AM, Hartline DK (2016) Evolution of rapid nerve conduction. Brain Res 1641:11–33.

Chiu SY, Ritchie JM (1980) Potassium channels in nodal and internodal axonal membrane of mammalian myelinated fibres. Nature 284:170–171.

Chiu SY, Ritchie JM (1981) Evidence for the presence of potassium channels in the paranodal region of acutely demyelinated mammalian single nerve fibres. J Physiol 313:415–437.

Devaux J, Alcaraz G, Grinspan J, Bennett V, Joho R, Crest M, Scherer SS (2003) Kv3.1b is a novel component of CNS nodes. J Neurosci 23:4509–4518.

Devaux JJ, Kleopa KA, Cooper EC, Scherer SS (2004) KCNQ2 is a nodal K^+ channel. J Neurosci 24:1236–1244.

Devaux JJ, Odaka M, Yuki N (2012) Nodal proteins are target antigens in Guillain-Barré syndrome. J Peripher Nerv Syst 17:62–71.

Enyedi P, Czirjak G (2010) Molecular background of leak K^+ currents: two-pore domain potassium channels. Physiol Rev 90:559–605.

Goldstein SA, Bayliss DA, Kim D, Lesage F, Plant LD, Rajan S (2005) International Union of Pharmacology. LV. Nomenclature and molecular relationships of two-P potassium channels. Pharmacol Rev 57:527–540.

Halter JA, Clark JW Jr (1993) The influence of nodal constriction on conduction velocity in myelinated nerve fibers. Neuroreport 4:89–92.

Hille B (1967) The selective inhibition of delayed potassium currents in nerve by tetraethylammonium ion. J Gen Physiol 50:1287–1302.

Hodgkin AL, Huxley AF (1952) A quantitative description of membrane current and its application to conduction and excitation in nerve. J Physiol 117:500–544.

Hodgkin AL, Katz B (1949) The effect of temperature on the electrical activity of the giant axon of the squid. J Physiol 109:240–249.

Hucho F, Bergman C, Dubois JM, Rojas E, Kiefer H (1976) Selective inhibition of potassium conductance in node of Ranvier with a photoaffinity label derived from tetraethylammonium. Nature 260:802–804.

Huxley AF, Stampfli R (1949) Evidence for saltatory conduction in peripheral myelinated nerve fibres. J Physiol 108:315–339.

Kanda H, Ling J, Tonomura S, Noguchi K, Matalon S, Gu JG (2019) TREK-1 and TRAAK are principal K(+) channels at the nodes of Ranvier for rapid action potential conduction on mammalian myelinated afferent nerves. Neuron 104:960–971.e967.

Kanda H, Tonomura S, Dai Y, Gu JG (2021a) Protocol for pressure-clamped patch-clamp recording at the node of Ranvier of rat myelinated nerves. STAR Protoc 2:100266.

Kanda H, Tonomura S, Gu JG (2021b) Effects of cooling temperatures via thermal K2P channels on regeneration of high-frequency action potentials at nodes of Ranvier of rat Abeta-afferent nerves. eNeuro 8: ENEURO.0308-21.2021.

Kang D, Choe C, Kim D (2005) Thermosensitivity of the two-pore domain K^+ channels TREK-2 and TRAAK. J Physiol 564:103–116.

Kim Y, Bang H, Gnatenco C, Kim D (2001) Synergistic interaction and the role of C-terminus in the activation of TRAAK K^+ channels by pressure, free fatty acids and alkali. Pflugers Arch 442:64–72.

Lillie RS (1925) Factors affecting transmission and recovery in the passive iron nerve model. J Gen Physiol 7:473–507.

Lotshaw DP (2007) Biophysical, pharmacological, and functional characteristics of cloned and native mammalian two-pore domain K^+ channels. Cell Biochem Biophys 47:209–256.

Maingret F, Patel AJ, Lesage F, Lazdunski M, Honore E (1999) Mechano- or acid stimulation, two interactive modes of activation of the TREK-1 potassium channel. J Biol Chem 274:26691–26696.

Maingret F, Lauritzen I, Patel AJ, Heurteaux C, Reyes R, Lesage F, Lazdunski M, Honore E (2000) TREK-1 is a heat-activated background K(+) channel. EMBO J 19:2483–2491.

Ranvier LA (1871) Contributions à l'histologie et à la physiologie des nerfs périphériques. Comptes Rendus Acad Sci 73:1168–1171.

Ranvier L (1872) Recherches sur l'histologie et la physiologie des nerfs. Archive de physiologie normale et pathologique 4:129–149.

Rasband MN, Trimmer JS, Schwarz TL, Levinson SR, Ellisman MH, Schachner M, Shrager P (1998) Potassium channel distribution, clustering, and function in remyelinating rat axons. J Neurosci 18:36–47.

Rhodes KJ, Strassle BW, Monaghan MM, Bekele-Arcuri Z, Matos MF, Trimmer JS (1997) Association and colocalization of the Kvbeta1 and Kvbeta2 beta-subunits with Kv1 alpha-subunits in mammalian brain K^+ channel complexes. J Neurosci 17:8246–8258.

Shibasaki K, Murayama N, Ono K, Ishizaki Y, Tominaga M (2010) TRPV2 enhances axon outgrowth through its activation by membrane stretch in developing sensory and motor neurons. J Neurosci 30:4601–4612.

Stathopoulos P, Alexopoulos H, Dalakas MC (2015) Autoimmune antigenic targets at the node of Ranvier in demyelinating disorders. Nat Rev Neurol 11:143–156.

Tasaki I (1939) The electro-saltatory transmission of the nerve impulse and the effect of narcosis upon the nerve fiber. J Physiol Lond 127:211–227.

Waddell PJ, Lawson SN (1990) Electrophysiological properties of subpopulations of rat dorsal root ganglion neurons in vitro. Neuroscience 36:811–822.

Waxman SG (1992) Demyelination in spinal cord injury and multiple sclerosis: what can we do to enhance functional recovery? J Neurotrauma 9 Suppl 1:S105–S117.

Waxman SG (2006) Axonal conduction and injury in multiple sclerosis: the role of sodium channels. Nat Rev Neurosci 7:932–941.

Zimmermann K, Leffler A, Babes A, Cendan CM, Carr RW, Kobayashi J, Nau C, Wood JN, Reeh PW (2007) Sensory neuron sodium channel Nav1.8 is essential for pain at low temperatures. Nature 447:855–858.